KTH ROYAL INSTITUTE
OF TECHNOLOGY

Degree Project in Chemical Engineering

Second Cycle, 30 Credits

Enhancing Mineral Carbonation of Olivine with CO_2

An Experimental Study on Particle Size and Assessment of the CO_2 Dissolution Rate through the Overall Mass Transfer Coefficient (k_La)

IKAROS ALTANTZIS

Stockholm, Sweden 2023

For the completion of my Masters dissertation project in Chemical Engineering for Energy and Environment at KTH, I conducted experiments in the pilot plant of Paebbl AB in Rotterdam, Netherlands.

Enhancing Mineral Carbonation of Olivine with CO_2

An Experimental Study on Particle Size and Assessment of the CO_2 Dissolution Rate through the Overall Mass Transfer Coefficient (kLa)

IKAROS ALTANTZIS

Master's Programme in Chemical Engineering for Energy and Environment

Date: 2023-06-14

Supervisors: Christophe Duwig, Pol Knops

Examiner: Christophe Duwig

School of Engineering Sciences in Chemistry, Biotechnology and Health (CBH)

Host company: Paebbl AB

Swedish title: Förbättring av mineral kolsyrning av olivin med CO_2

Swedish subtitle: En experimentell studie på partikelstorlek och bedömning av CO_2-upplösningshastighet en genom den totala massöverföringskoefficienten (kLa).

Abstract

Carbon dioxide (CO_2) emissions from the energy production industry and the transportation sector globally negatively affect the environment. A prominent example is the interconnection of carbon with the greenhouse effect. Countries have agreed to mitigate their emissions and try to fulfill the target of 1.5 ^oC average temperature increase by 2030, but in order to do so the global emissions of CO_2 from fossil fuels and industrial processes will still lead up to the astonishing amount of 40 Gtons of CO_2 each year until 2100.

It is apparent that processes that try to take advantage of the emitted CO_2 creating valuable products with negative emissions are highly desired. One of these is mineral carbonation, where CO_2 and minerals dissolve in an alkaline solution and form stable products. Many factors affect the rate at which mineral carbonation happens. The effect of the particle size of the mineral in the process will be investigated, along the CO_2 dissolution rate through the overall gas-liquid mass transfer coefficient (k_La), in order to get a better understanding of the process.

Experiments were conducted with a batch reactor provided by Paebbl AB and a mathematical model was developed in Matlab. The experimental and numerical results, in regards to the particle size, were then compared for the cases of three resistances. This model can be developed further for use in a continuous mineralization process. The results revealed that increasing the particle size of olivine leads to a significant increase in the time required for total conversion, irrespective of the resistance type. The modelled resistances were found to inadequately describe the process, suggesting a simultaneous and uniform effect of all three resistances on olivine mineralization, in addition to the effect of other possible limitations such as impurities and by-products. Mineralization experiments with 20μm particles and a duration of 1 hour led to 34.4% conversion, whereas experiments with 10μm particles and a duration of 2 hours resulted in 46.7% conversion. Finally, the initial investigation of the mass transfer limitations in a system of CO_2 and water led to an average k_La coefficient of 191 h^{-1}, suggesting that the CO_2 dissolution rate is not the limiting factor. However, the impact of lower stirring rates remains unexplored due to the absence of appropriate instrumentation and the behaviour of the (CO_2 + olivine) system should also be studied. Future research should aim to address these limitations.

Keywords

CO_2 sequestration, Dissolution rate, Kinetics, Mineral carbonation, Olivine, Particle size

Sammanfattning

Koldioxidutsläpp (CO_2) från energiproduktionsindustrin och transportsektorn globalt påverkar miljön negativt. Länder har enats om att minska utsläppen för att nå målet om en genomsnittlig temperaturökning på 1,5 °C till 2030. Trots detta förväntas de globala utsläppen av CO_2 från fossila bränslen och industriella processer vara cirka 40 Gton per år fram till 2100.

För att dra nytta av CO_2-utsläppen och skapa värdefulla produkter med negativa utsläpp är mineralkarbonatisering en önskvärd process. Denna process innebär att CO_2 och mineraler löses upp i en alkalisk lösning och bildar stabila produkter. Faktorer som partikelstorlek hos mineralerna och CO_2-lösningshastigheten påverkar mineralkarbonatiseringens hastighet.

Experiment utfördes med en batchreaktor från Paebbl AB och en matematisk modell utvecklades i Matlab. Resultaten jämfördes för olika partikelstorlekar i tre motståndsfall. Större partikelstorlek hos olivin visade sig öka tiden för total konvertering, oavsett motståndstyp. De modellerade motstånden beskrev inte tillräckligt processen och indikerade att alla tre motstånd har en samtidig och enhetlig effekt på olivinmineralisering, utöver eventuella begränsningar som föroreningar och biprodukter. Mineraliseringsexperiment med 20 µm partiklar under en timme gav 34,4% omvandling, medan 10 µm partiklar under två timmar gav 46,7% omvandling. En inledande undersökning av massöverföringsbegränsningar visade att CO_2-lösningshastigheten inte är den begränsande faktorn, utan lägre omrörningshastigheter och beteendet hos (CO_2 + olivin)-systemet behöver ytterligare studeras. Framtida forskning bör fokusera på att lösa dessa begränsningar.

Nyckelord

CO_2-inlagring, Upplösningshastighet, Kinetic, Mineral kolsyrning, Olivin, Partikelstorlek

Acknowledgments

I would like to express my outmost gratitude to every party involved that helped me complete my Masters dissertation. I would like to thank Professor Christophe Duwig at KTH for giving me the opportunity to conduct such an interesting research project and contribute towards a more sustainable future. His feedback was always helpful and constructive. I also want to thank Paebbl AB for letting me use their intellectual property for my experiments. I am also very grateful to my supervisor Pol Knops from Paebbl AB, who provided me with many much needed data and supported me throughout my dissertation. Our prompt communication with Pol Knops and Prof. Christophe Duwig as well, made it possible to clear out any questions that I had and correct mistakes along the way. I would like to extend my gratitude to Marta Sjögren and Andreas Saari for believing in me and choosing me to be part of this journey. Prof. Wim van Swaij from University of Twente, Netherlands also deserves acknowledgement for being a very valuable advisor for this project. His involvement in the project was highly appreciated and his advice proved to be exceptional. Finally, I would like to thank my family for their continuous support.

Stockholm, June 2023
Ikaros Altantzis

List of Abbreviations

BR – Batch Reactor

CCS – Carbon Capture and Storage

CCU – Carbon Capture and Utilization

CSTR – Continuous Stirred Tank Reactor

EGR – Enhanced Gas Recovery

LCA – Life Cycle Assessment

LOI– Loss on Ignition

RTD – Residence Time Distribution

PFR – Plug Flow Reactor

SCM – Shrinking Core Model

SOP – Standard Operating Procedure

SPM – Shrinking Particle Model

STR – Stirred Tank Reactor

TRL – Technology Readiness Level

List of Figures

Table of Contents

1. Introduction

Greenhouse gases such as carbon dioxide (CO_2) are responsible for global warming. Normally, part of the light from the sun (radiant energy) is absorbed by the Earth's surface and the rest is reflected. When carbon dioxide is released into the atmosphere though, some of the reflected energy is absorbed by CO_2 molecules or other particles and this results in entrapment of heat, thus increasing the temperature [1]. Of course, global warming is just the tip of the iceberg and triggers a chain reaction of many negative effects such as the melting of ice glaciers, sea level rise and endangerment of natural ecosystems and human society [2].

1.1 Background

Global warming is not something new. The effect of CO_2 on global temperature has been studied extensively for centuries and some insight on the matter is provided in Figure 1 below.

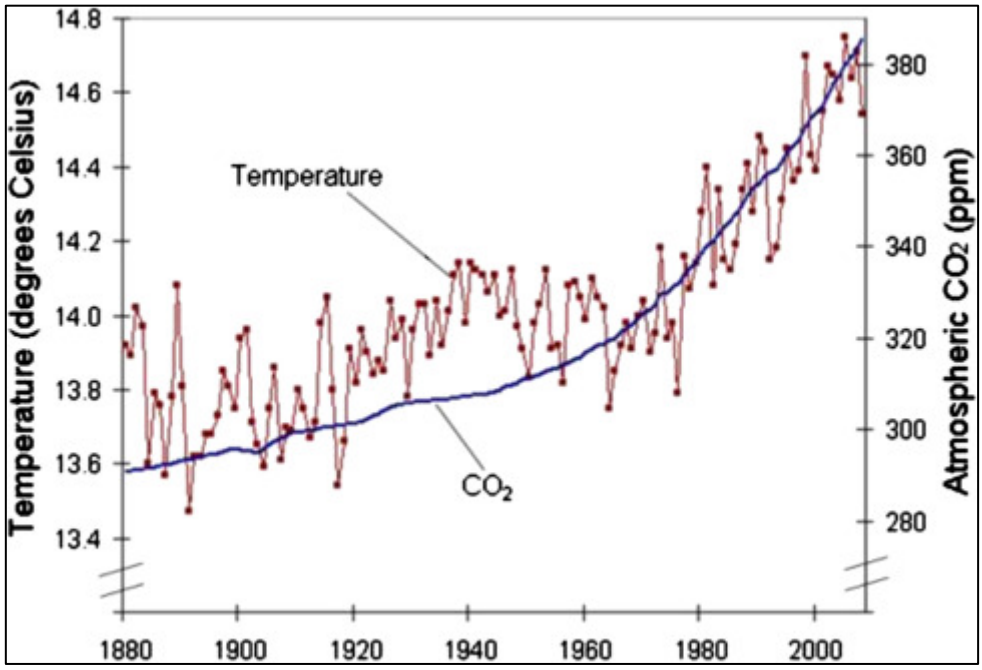

Figure 1. Correlation between increase of global temperature and atmospheric levels of CO_2 [1]

The 20th century has been marked by anthropogenic activities that led to an increase of greenhouse gas emissions into the atmosphere. These were mainly the exploitation of fossil fuels [3]. Unfortunately, the trend does not seem to stop with new record-breaking levels of

CO_2 being recorded in the atmosphere every year. It is only in the past few years that actions have started being implemented on a universal scale to combat climate change. The most prominent examples are the Paris Agreement and the European Green Deal that were signed in 2016 and 2019 respectively [4, 5]. By taking a closer look on these treaties though, it becomes apparent that the measures stated in these only aim to reduce CO_2 emissions by at least 55% by 2030 and reach net-zero carbon emissions by 2050. Until then, emissions of greenhouse gases will still occur, thus increasing the global temperature even further. Nonetheless, when exploring the scenarios presented in the Paris Agreement, there is an excess of 40 Gtons of CO_2 that will be emitted in the following decades from industries and burning of fossil fuels, even when trying to fulfil the target of 1.5 ºC average temperature increase by 2030 [4].

Scientists have issued warnings that, if the levels of CO_2 keep increasing, it could lead to irreversible climate change [3]. This dire situation and need for change sparked profound interest in the science society to find new ways to mitigate the negative effects of climate change with methods producing negative emission materials being highly desired. Research led to the development of novel methods that can be categorized in two fields. These are Carbon Capture and Storage (CCS) and Carbon Capture Utilization (CCU). Figure 2 provides an overall scheme of carbon capture and the respective main methods involved in each case.

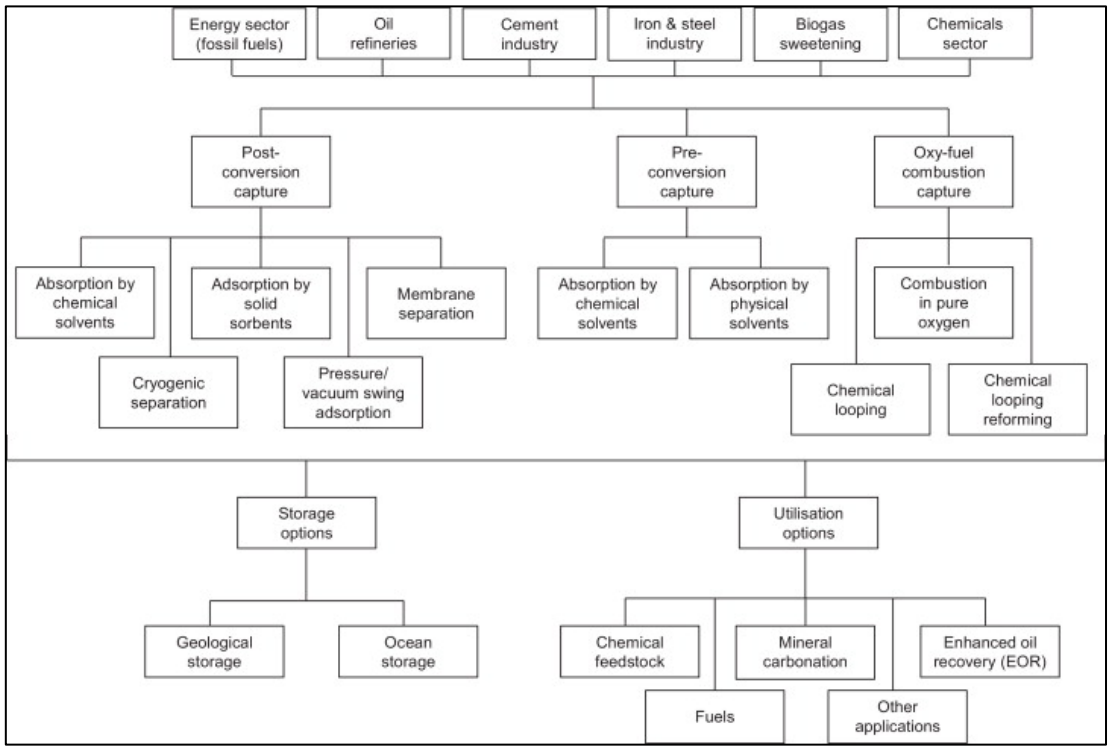

Figure 2. Main methods in the fields of CCS and CCU [6].

In the field of Carbon Capture and Storage (CCS) a stream of carbon dioxide that usually derives from industrial sources is treated and transported to a location for long-term storage. This technology is considered crucial for reducing greenhouse gas emissions and combating climate change, while taking cost-effectiveness into account [7, 8]. It must be noted that Figure 2 provides a brief overview of carbon capture methods and storage options and that there are many other available. Two examples would be the storage of CO_2 by enhanced gas recovery (EGR) and storage in depleted gas and oil fields [8]. In the case of EGR, CO_2 is injected in underground reservoirs of crude oil that could not be otherwise extracted, thus displacing it. The gas injection of CO_2 basically increases the ability of oil to flow [9]. Of course, this crude oil can then be used for fuel production that will release new CO_2 emissions into the atmosphere. Unfortunately, most of the available methods of carbon storage such as ocean storage have not reached commercial stage yet and are only being implemented on a smaller scale due to lower technology readiness level (TRL) [8]. On the other hand, the carbon capture methods that have reached commercial stage are geological storage, saline formations and CO_2-enhanced oil recovery (EOR), but they will not be discussed further as it is beyond the scope of this thesis.

Nonetheless, the success of a CCS project is always interconnected with the availability of safe geological storage. It is possible that the stored CO_2 could seep into various pathways such as wells, geological faults or fractures. This could result in the movement of CO_2 into shallow geological formations or even into the atmosphere. The potential of contaminating underground water, soil, rivers and air would be high and such a contamination could very well cause harm to the ecosystem and pose a risk to human health as well [8, 10].

It becomes apparent that CCS – although beneficial – provides a short-term solution to the problem of greenhouse gas emissions, since there is no permanent CO_2 removal taking place. Additionally, the implementation of CCS technologies – but also that of CCU – is currently accompanied by high energy requirements and initial investment cost (CAPEX, OPEX) [11].

The second innovative field, Carbon Capture Utilization (CCU) is fairly new compared to CCS, is growing rapidly and can be a long-term solution to the problem. It consists of processes designed to capture carbon dioxide (CO_2) emissions that are generated from industrial processes and reuse them in various applications such as fertilizer or ammonia production. [6]. Captured CO_2 comes from industrial activities such as fossil-fuelled power plants and refineries before it is released in the atmosphere and is mainly used as a raw material for chemicals and fuels production, thus reducing the levels of CO_2 in the atmosphere. It is apparent that CCS and CCU are not synonymous, since CCU does not intend to permanently store carbon dioxide underground [12]. The concept of CCU, similarly to CCS, is relatively premature, because

although the stages of CO_2 capture, transportation, utilization and storage are known, combining these components together successfully is complicated and they have never been united as a system previously [13]. This might scare off potential investors or parties involved, but it is balanced out by the fact that CCU has the potential to create economic opportunities by providing new revenue streams from value-added end products for industries that produce carbon emissions and most importantly, mitigate the negative effects of climate change bringing the globe closer to a sustainable future.

Two characteristic examples of CCU applications are the transformation of captured CO_2 into alcohols, such as methanol, that can be used as a biofuel or its transformation in commercial products such as plastics or reactants for various chemical processes [12]. Even on this case though, CO_2 emissions will re-enter the atmosphere at some point. Another option is biological fixation, where algae and plants are utilized to absorb CO_2 and convert it to biomass [14, 15].

Mineralization is the final process included in the CCU field and perhaps the most promising one. More specifically, carbon mineralization can be described as the process by which carbon dioxide is converted into solid inorganic carbonates (minerals) [16]. Mineralization is one of the few processes in CCU where an exothermic reaction takes place and therefore does not require a large input of energy [17]. It must be noted that CO_2 mineralization is a process that occurs naturally, although slowly. Presence of CO_2 in water or moist air causes hydrolysis and leads to sequestration of about 30 Gt of CO_2 from the atmosphere each century into rocks, thus changing their molecular structure (chemical weathering) [18].

In general, resources containing Calcium (Ca^{2+}) or Magnesium (Mg^{2+}) are needed for mineralization leading to calcium and magnesium carbonates respectively [16]. Magnesium oxide-based silicates though are abundant in nature and as a result they are favoured for the mineralization process. More specifically, two subgroups of magnesium silicates are preferred due to the large amounts available. These are olivine $(Mg,Fe)SiO_4$ and serpentine $(Mg_3Si_2O_5(OH)_4)$ [19]. The produced minerals are practically stable and the thermodynamic mechanism will be discussed later on. This means that the captured CO_2 cannot escape back into the atmosphere.

Since the process is thermodynamically downhill, CO_2 sequestration is attractive to be industrialized and utilized for production of enhanced products or replacement of existing ones. The use of CO_2 in industrial processes though is limited, but not something entirely new. It first started being used in the 18th century for carbonating beverages, for accelerating the hardening of cementitious materials (19th century) and more recently for producing pharmaceuticals and constructing materials [18]. Based on literature data, the second most produced product

globally, after clean water, is concrete. For each tonne of cement used in it, approximately 880 kg of CO_2 are emitted into the atmosphere. As a result, cement production is responsible for 5% of global CO_2 emissions [8].

For cement production, the main material is usually limestone ($CaCO_3$), which causes high CO_2 emissions when it reacts, but can be produced by mineral carbonation. Concrete is produced by mixing water, cement and aggregates such as sand. If CO_2 is added to the mixture, then the cement reacts with it, resulting in mineralization and permanent storage inside the concrete. Essentially in this case, concrete can be seen as a liquid rock that transforms CO_2 into stone [20]. Thus, through mineralization by using CO_2 as a feedstock, carbonated concrete can be produced, which can subsequently replace traditional concrete in construction projects. This process not only reduces carbon emissions, but also produces a more sustainable building material with negative carbon footprint.

It is apparent that there are plenty of commercial opportunities for mineralization that can even involve mineralization of wastes to remove them from landfill and convert them into products with added value. Changes in commercial environments and regulations are bound to happen though and must be followed by life-cycle assessments (LCA) to confirm that the process is viable. Other challenges that CCU faces in general, include the high cost of technology and the need for further research and development. The technology is still in its early stages and requires significant investment to become commercially viable. Additionally, the availability of carbon capture technologies and the accessibility of CO_2 sources vary significantly by region, making it difficult to implement CCU on a large scale [18].

With that being said, carbon capture and utilization (CCU) remains still a promising technology that has great potential to reduce carbon emissions, while generating economic benefits. By converting CO_2 emissions into useful products, CCU offers a more sustainable solution to climate change, unlike traditional carbon capture and storage (CCS). Nevertheless, additional research and development are required in order to make CCU more cost-effective and scalable. As the globe continues to face the challenges of climate change, CCU, and more importantly CO_2 mineralisation, represent an important step towards the creation of a more sustainable future.

.

1.2 Aim and Objectives

The aim of this study is to investigate the process of mineral carbonation of olivine with CO_2 in a batch reactor (BR) both experimentally and within a simulation environment that is solved numerically, by introducing an appropriate reaction model where the degree of conversion is calculated. The derived results will be compared between different particle sizes and suggestions for optimisation will be provided. Reaction limitations, such as mass transfer and diffusion, which depend on parameters such as pressure and temperature, are also of interest.

The main objective of the project is that an analysis of the results, in addition to a written master thesis, is carried out, reported together with the state-of-the-art and with the student showing mastery of knowledge on the topic.

The three main research questions being investigated and answered are:

How does the particle size affect the conversion of olivine during the process carbonation of olivine with CO_2 in a batch reactor in a simulation environment?

Are numerical and experimental results in regards to olivine conversion comparable? If not, why?

How does the CO_2 dissolution rate vary under different conditions? Is it fast enough?

1.3 Delimitations

The delimitations of this study are as follows:

- The project focuses on CO_2 mineralization with olivine as the raw material. Analysis and experiments using other raw materials is omitted.
- The process of CO_2 mineralization has not been investigated thoroughly yet and the effect of many parameters remains unknown. Furthermore, the thesis has been conducted in collaboration with Paebbl AB and contains background literature that is confidential and cannot be fully shared, thus limiting the scope of the project.
- No energy survey for the process has been performed due to limited data available.

1.4 Assumptions

This paragraph focuses on the main assumptions that were necessary during this project and presents short descriptions for each one in the form of a Table below.

Table 1. Required assumptions for this project

Assumption	Description
Raw material is pure olivine	Without impurities there are no spatial or temporal variations in density and reaction rate
Spherical particles of olivine of constant size	The Shrinking Core Model (SCM) can be applied
Reaction occurs across a sharp front between raw material and product and not along a diffuse front	SCM can be applied
Raw material is little porous	SCM becomes more applicable compared to other models, e.g. Continuous Reaction Model
No temperature gradients within the particles	Reaction rate is uniform around the particle and SCM can be applied
Reaction occurs at operating temperature	Minimal conversion that can happen during the heat-up of the reactor can be omitted
Concentration of CO_2 at the gas side of the gas-liquid interface is equal to bulk concentration of CO_2 in solution	Eliminates transfer resistance within gas-liquid interface

2. Technical Background

In this chapter, a more detailed depiction of the mineral carbonation process is presented. Mineralization is dependent on many parameters, some of which are beyond the scope of this project. The focus will remain on some key factors that play a role in the process. Mineral and CO_2 dissolution are discussed, followed by a presentation of parameters that can increase the rate of the process. Additionally, a section explaining the chemical reaction is included in this chapter and the reaction models that were implemented in this project follow. For a more detailed description of these, please refer to Appendix A. Finally, the simulation software that was used during this project is explained.

2.1 Minerals

The term "mineral" is used for every naturally occurring solid compound that has distinctive chemical and physical properties, crystal structure and chemical composition [21]. During mineral carbonation, CO_2 is fixated by using a suitable feedstock, such as alkaline and alkaline-earth oxides. Such oxides are calcium oxide (CaO) and magnesium oxide (MgO). These oxides are present as naturally occurring silicate rocks. A type of silicate rock that contains calcium oxide is wollastonite, whereas a silicate rock that contains magnesium oxide is olivine or serpentine [22]. It is thus apparent that even alkaline waste materials are suitable for mineralization, one of the being cement kiln waste [23]. This project focused on the mineral carbonation of CO_2 with olivine.

2.1.1 Olivine

Olivine ($(Fe,Mg)_2SiO_4$) is a silicate that usually appears with an unusual green colour of the magnesium-iron olivine series [24]. It has great potential for use in mineral carbonation since it is abundant in nature and has a widespread distribution in various geographical locations. Olivine is environmentally friendly and poses no threat to human health, but it reacts less rapidly compared to other minerals such as wollastonite. To put into perspective the abundancy of olivine, fixation of CO2 from all coal plants globally could be achieved by olivine and olivine reservoir tanks would still be available for exploitation [25, 26].

2.2 Dissolution of Olivine and Effect of Parameters

Before olivine can be used in the process of CO_2 sequestration it must be dissolved in a solution. This is because under ambient conditions, mineral carbonation takes place extremely slow [27]. Due to this reason the reaction has to be sped up, if the carbon sequestration process is to become environmentally and economically viable. When it comes to mineral dissolution, there are many factors that come into play in regards to rate improvement of the process. Among the most important ones are temperature, pH, ions presence and, in the case of olivine, the amorphous silica layer that impedes the rate of mineral dissolution and reaction [28]. The amorphous silica layer, although presenting unique interest, is beyond the scope of this project and not investigated due to time constraints.

2.2.1 Mechanism of Mineral Dissolution

Magnesium is the main alkaline metal contained in olivine and it can be leached by proton activity. This means that magnesium undergoes a chemical reaction due to interaction of protons. This can be visualized by the following reaction [29]:

$$Mg_2SiO_4 + 4H^+ \rightarrow 2Mg^{2+} + SiO_2 + H_2O \quad (2.1)$$

According to the literature [30], the leaching process of magnesium cations (Mg^{2+}) from olivine that is not yet converted, exactly like in the case of wollastonite mineral (Ca^{2+}), can be separated into three stages. The first step involves the diffusion of protons (H^+) through the silica layer on the particle surface towards the unconverted olivine core. The diffusion of protons affects the pH of the solution, which is a measurement determining how acidic or basic a solution is [31]. The second step is characterized by the release of magnesium from the olivine structure matrix, which leaves solid silica as a by-product. The third and final step consists of the diffusion of magnesium cations, where H_2O is a by-product, through the silica layer, moving towards the solid/liquid interface. The magnesium cations can thereby react with carbonates at this solid-liquid interface or in the bulk solution leading to the formation of magnesite [32].

2.2.2 Effect of Temperature

The dissolution rate of olivine increases as temperature is increased [32]. Nonetheless, the effect of temperature is two-fold. Based on the Van't Hoff equation of the Henry constant for carbon dioxide, which will be explained in detail later on, the temperature cannot be increased indefinitely to boost the mineral dissolution. The reason for this is that the solubility of carbon

dioxide decreases at higher temperatures. It is obvious that these two phenomena are acting in opposition to each other and as a result, there is an optimum temperature of operation, which is different for each kind of mineral. In the case of olivine, the optimal temperature for the carbonation process is 175 ºC [25]. With that being said, pressure can also be adjusted to boost the rate, since increasing CO_2 pressure leads to higher solubility of CO_2, although temperature is a more important parameter.

2.2.3 Effect of pH

By taking a look at the leaching reaction of the main component of olivine (Eq. 2.1), it becomes apparent that if the solution becomes more acidic, this corresponds to an increase of proton concentration and these extra protons lead to a higher removal of Mg^{2+} ions from the structure of olivine. This is also backed up by the Le Chatelier principle [33]. One way to decrease the pH of the solution is by increasing CO_2 pressure. This will become clearer in the following sections, where the mechanism of carbon dioxide dissolution will be explained.

2.2.4 Effect of Ions

It was mentioned before that the mineral dissolution rate can be increased by lowering the pH (more acidic). At some point though, the pH is so low that even the formed carbonate is dissolved. This value of pH varies depending on the kind of carbonate [33]. Literature studies have shown that there is a specific range of pH values that favour carbonation, which can be achieved by adding a buffer agent, $NaHCO_3$, which keeps the solution pH within that range. Essentially, $NaHCO_3$ acts as a catalyst [34].

2.3 Dissolution of Carbon Dioxide and Effect of Parameters

2.3.1 Mechanism of Carbon Dioxide Dissolution

In order for carbon dioxide to react with forsterite (Mg_2SiO_4) it must dissolve in water. To do so, carbon dioxide has to be transferred from the bulk of the gas to the gas-liquid interface and diffuse through the liquid film into the bulk of the liquid. For faster and more efficient dissolution, the area in the gas-liquid interface (interfacial area, a) has to be increased. Smaller bubbles of carbon dioxide correspond to more surface area per unit volume and as a result, the interfacial area for mass transfer is increased. The concentration of dissolved carbon dioxide is

correlated with its partial pressure above the solution by Henry's Law and Henry's constant, k_H, which is temperature-dependent [35].

It is important to mention that the interfacial area is part of a term called overall mass transfer coefficient (k_La), which determines the rate at which a gas transfers between the gas and the liquid phase [36]. The mineral carbonation reaction might not be reaction controlled – at least under specific conditions – but mass transfer limited by the kLa. This represents one of the key questions of the dissertation that will be investigated and will be explained thoroughly throughout the following chapters.

2.3.2 Effect of Temperature

The temperature dependence of Henry's Law constant can be expressed as a form of the Van't Hoff equation as [37]:

$$k_H(T) = k_{H,298K} * exp\left[-C * \left(\frac{1}{T} - \frac{1}{298}\right)\right] \quad (2.2)$$

Where:

$k_H(T)$ = Henry's constant at a specific temperature T in Kelvin, [Pa*m^3/mol]

$k_{H,298K}$ = Henry's constant at 298 K (25 ^{o}C), [Pa*m^3/mol]

C = constant which is specific for each gas, [K]

Henry's Law states that the amount of a dissolved gas, in this case CO_2, in a liquid is directly proportional to its partial pressure and is given by the following equation [38]:

$$C_{sol,CO_2} = k_{H,CO_2} * P_{CO_2,g} \quad (2.3)$$

With these two Equations, and values for the CO_2 constants [35], the solubility of carbon dioxide in water can be calculated for a wide range of temperatures and pressures.

2.3.3 Effect of pH

In order to better understand the influence of pH on the dissolution of carbon dioxide, the reaction pathway of CO_2 has to be explained.

$$CO_2 + H_2O \leftrightarrow H_2CO_3 \quad (2.4)$$

$$H_2CO_3 \leftrightarrow H^+ + HCO_3^- \ (\leftrightarrow 2H^+ + CO_3^{2-}) \quad (2.5)$$

$$HCO_3^- \leftrightarrow H^+ + CO_3^{2-} \quad (2.6)$$

At first, carbon dioxide reacts with water and forms carbonic acid. Afterwards, carbonic acid dissociates twice. From this reaction path it becomes evident that there is an equilibrium between carbonic acid and protons. The lower the pH of the solution, the more protons that are present, which then drive the reaction towards the undissociated side. Consequently, this impedes carbonation, since less carbonic ions are readily available. Nonetheless, the pH is mainly affected by the dissolution of carbon dioxide, when high pressure is applied. Increasing the partial pressure of CO_2 though, can have adverse effects for carbonation. By increasing the partial pressure of CO_2 pressure, more bicarbonate will dissolve, thus lowering the pH. At some pH the carbonate starts to dissolve and the reaction is shifted backwards. Similar to temperature, an optimum pressure can also be determined for the mineralization process.

2.4 Chemical Reaction of Carbonation

2.4.1 Mechanism

In the case of mineralization, the overall reaction pathway can be written thoroughly as:

$$CO_2 + H_2O \leftrightarrow H_2CO_3 \quad (2.4)$$

$$H_2CO_3 \leftrightarrow H^+ + HCO_3^- \ (\leftrightarrow 2H^+ + CO_3^{2-}) \quad (2.5)$$

$$HCO_3^- \leftrightarrow H^+ + CO_3^{2-} \quad (2.6)$$

$$\frac{1}{2}\, Mg_2SiO_4 + 2H^+ \leftrightarrow Mg^{2+} + H_2O + \frac{1}{2}\, SiO_2 \quad (2.7)$$

$$Mg^{2+} + CO_3^{2-} \leftrightarrow MgCO_3 \quad (2.8)$$

As discussed before, the CO_2 dissolution rate is affected by pH. Protons take part in the first four steps of the reaction path and different amount of each carbon species exists for every

pH value. For example, for pH values lower than 4, carbonic acid is almost exclusively present, whereas at pH=8 and pH>12 there is a maximum of HCO_3^- and CO_3^{2-} ions, respectively [39].

Many models exist to solve complex problems. For this case, an applicable model would be the Shrinking Core Model (SCM). Of course, the carbonation rate might be reaction rate limited or mass transfer limited and these cases will be investigated in the following chapters.

2.4.2 Thermodynamics

Figure 3 shows the possibilities of carbon utilization accompanied by the associated energy state.

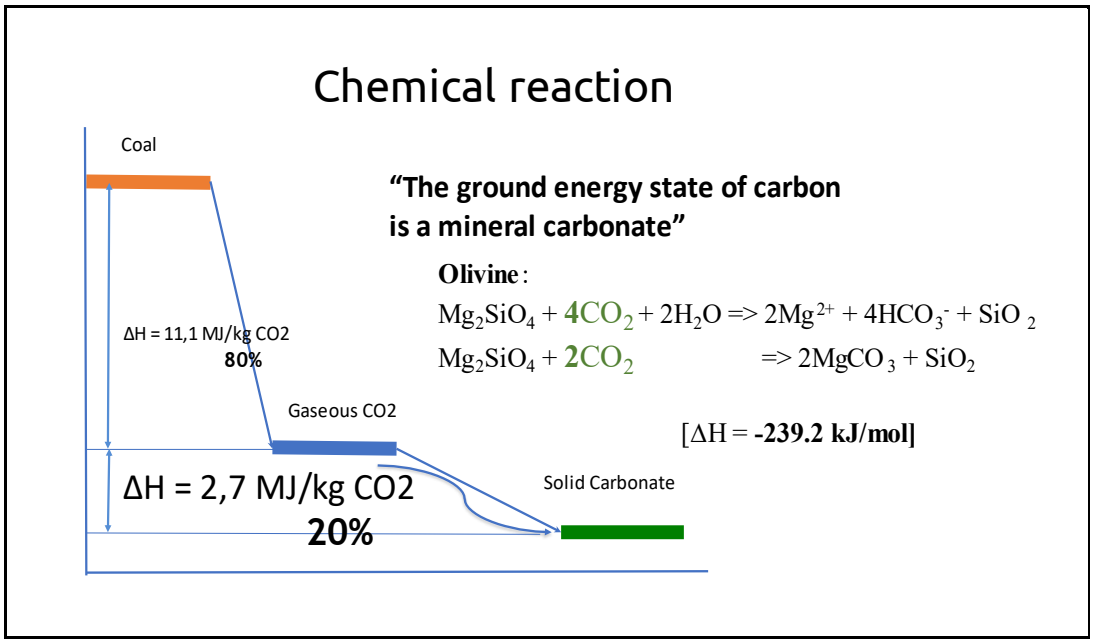

Figure 3. Conventional CCS energy requirements and energy state for carbonation [Courtesy of Pol Knops, Green Chemicals]

The olivine mineralization reaction can be expressed per 1 mol of CO_2 as [40]:

$$CO_2 + \frac{1}{2}\, Mg_2SiO_4 \rightarrow MgCO_3 + \frac{1}{2}\, SiO_2,\ \Delta H = -88\ \frac{kJ}{mol} \quad (2.9)$$

The reason that the conversion of carbon dioxide to a carbonate such as olivine is exothermal (indicated by the sign "-" in Reaction above) is because the carbonate form has the lowest level of energy that a carbon compound can achieve. This is verified also by Figure 3. As a result, the formation of carbonates is thermodynamically favoured and they tend to be

chemically stable and rather benign from an environmental point of view [41]. This is an important requirement for tackling the problem of the ever-increasing CO_2 emissions.

2.4.3 Overall Reaction Rate

From the analysis presented above, it is obvious that mineralization is a process that is affected by many parameters, some of which have an antagonizing effect, such as the pH. Although research has shown that the mineral dissolution reaction time can be reduced by using low pH [42], on the other hand, carbonate precipitation is boosted by higher pH values. Nonetheless, experiments have shown that both steps can be combined into one single step process [26]. The temperature and additives in the solution must be closely monitored, since carbon dioxide dissolution is also of great importance.

2.5 Reaction model

The Shrinking Core Model (SCM) is a useful tool to explain situations where solid particles are gradually being consumed, either due to dissolution or reaction. Consequently, there is a reduction in the amount of material, thus resulting in a "shrinking" effect [43]. It must be taken into account that the model's theory – as with the second model that will be explained in the next paragraph – was originally developed concerning the gas phase. Nonetheless, it can still be applied in the case of liquids although with different coefficients.

In the Shrinking Core Model in liquids, diffusion through the liquid is usually slower. Carbon dioxide is transferred from the gas phase into the liquid and it diffuses from the bulk liquid to the film around the liquid and it finally reaches and diffuses through the external silica layer of the particle, which is porous, towards the unreacted core where the chemical reaction occurs. The core is shrinking and the reaction comes to an end when the whole particle is converted. As the chemical reaction takes place, the products (carbonate and silica) precipitate around the unreacted core or diffuse through the product layer and silica and precipitate on the external surface of the particle. In each case for the SCM, it is assumed that the particle size is constant and the concentration of CO_2 in the bulk liquid is at equilibrium and equal to the gas concentration at the gas – liquid interface.

During mineral carbonation, where CO_2 is the gaseous reactant, the reaction is of the following type $aA(g) + bB(s) \rightarrow solid\ product$. In more detail, the SCM consists of five steps [43]:

- The first one is the diffusion of the gaseous reactant A through the liquid film, that is surrounding the particle, to the surface of the solid particle.
- The second one is the penetration and diffusion of reactant A through the area of product to the surface of the unreacted core.
- The third step consists of the reaction of A with the solid (unreacted core).
- The fourth step is the diffusion of gaseous products through the product layer back to the outer surface of the solid.
- The fifth and final step consists of the diffusion of the gaseous products through the liquid film.

This mechanism can be visualized in Figure 4 (shown for the case of a gas phase).

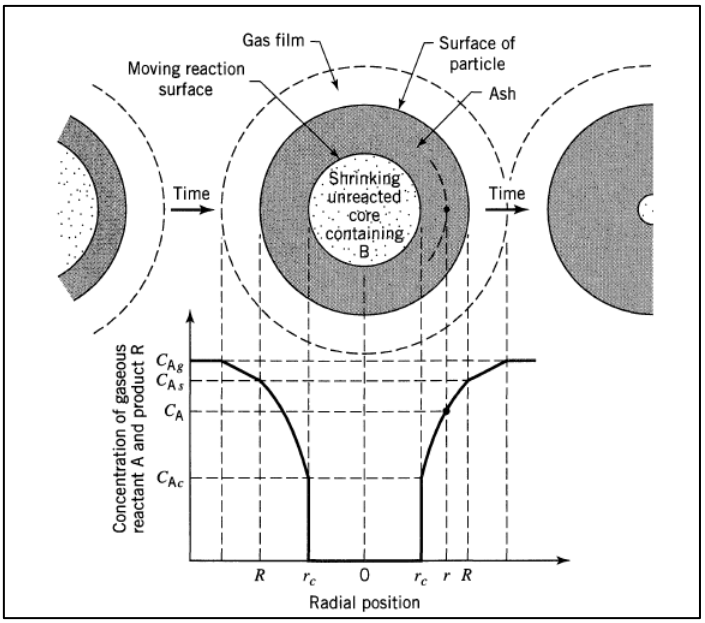

Figure 4. Shrinking core model for spherical particle and concentration profile of reactant [43]

It must be noted that the reaction can be limited by gas diffusion through the liquid film layer, by the reaction rate or by diffusion through the product layer. For each one of these cases the concentration profile in Figure 4 changes accordingly. This model has been used extensively in the literature and as an example, the equations used for the case of product layer diffusion resistance are presented below. All equations for each case are contained in the Matlab code.

Considering that the olivine reaction is irreversible with no gaseous products (Eq. 2.9), the last two steps that were presented for the mechanism of the shrinking core model can be

discredited as rate-determining. The assumption has been made that the particles are spherical (Table 1). One of the cases that will be modelled with the help of the simulating software is the shrinking core model with product layer diffusion control. Governing Equations for all cases were added in the simulation workspace. For the aforementioned case for example, based on the literature, two Equations are presented [43]:

$$\tau = \frac{\rho_B * R_p^2}{6 * b * C_{Ag} * D} \quad (2.10)$$

$$\frac{t}{\tau} = 1 - 3 * \left(\frac{R}{R_p}\right)^2 + 2 * \left(\frac{R}{R_p}\right)^3 = 1 - 3 * (1 - X_B)^{\frac{2}{3}} + 2 * (1 - X_B) \quad (2.11)$$

Where:

τ = time for complete disappearance of particle, [sec]

ρ_B = density of olivine, [kg/m^3]

R_p = initial radius of the particle, [m]

b = constant for the reaction (in this case b = 1), [–]

C_{Ag} = concentration of reactant A on surface of product layer (= bulk concentration of A in solution), [mol/m^3]

D = effective diffusivity coefficient (through product layer) of CO_2, [m^2/sec]

R = radius of the unreacted core, [m]

X_B = conversion of reactant B (in this case B = olivine), [–]

With the help of Equations 2.10 & 2.11, the conversion of olivine over time can be found when diffusion through the product layer is the rate-limiting step. With this relation known, the segregated model could be applied in future developments of the project in order to derive results for the case of a continuous stirred tank reactor (CSTR), which is useful when scaling up from a batch reactor (BR). A description of the segregated model and a mass balance will be presented in Chapter 2.7. It must be noted that in these cases, olivine is considered without impurities.

2.6 Residence Time Distribution (RTD)

The Residence Time Distribution can be defined as the probability distribution of the time that a molecule or group of molecules spend in the reactor. The particles entering a CSTR reactor for example, do not stay inside the reactor for the same duration. Part of them stay for a shorter duration than others. Molecules close to the wall move slower, because of friction and diffusion in the liquid that causes them to move backwards or forward.

RTD is of great importance when designing a process and during operation. The reason for this is because when the RTD function is well-defined, the process can be optimized. Different RTD functions have been developed for each case of reactor such as CSTR and Plug Flow Reactors (PFRs). One of the ways that the RTD function can be determined is by measuring the system response for a short tracer pulse and the tracer concentration at the exit (for a closed system) [43, 44, 45].

The RTD function has been investigated extensively and for the case of a CSTR, the following Equations are of importance. The mean residence time is given by:

$$\bar{\tau} = \frac{V}{F}\ [sec] \quad (2.13)$$

Where:

V = volume of the reactor, [m^3]

F = volumetric flow rate, [m^3/s]

In the case of a perfectly mixed CSTR, the RTD function is given by [44]:

$$E(t) = \frac{1}{\bar{\tau}} * e^{-\frac{t}{\bar{\tau}}} \quad (2.14)$$

Where $E(t)$ corresponds to the residence time distribution function (RTD), [s^{-1}].

2.7 Complete Segregation Model and Mass Balance for CSTR

As mentioned in Chapter 2.5.1, when considering the case of a CSTR, "perfect mixing" is not a good option and thus, a non-ideal approach is adopted. This produces results that are closer to the real-life case scenario. The reaction in this case is not simply first order and for this reason knowledge of RTD is not sufficient to calculate conversion. The degree of mixing of molecules is also of great importance in this case. The model that can be chosen to account for the mixing of molecules inside the CSTR reactor is the complete segregation model. Here, all molecules that fall into the same age group of the RTD function is assumed to stick together as they travel through the reactor. Mixing with other groups of molecules of different age groups occurs only at the exit of the reactor [44]. With the help of this model, a mean conversion of olivine exiting the reactor can be calculated. This will come in handy when developing the mass balance for the case of the CSTR reactor.

The mean conversion with the complete segregation model is given by [44]:

$$\bar{X} = \int_0^\infty X(t) * E(t)\, dt \quad (2.15)$$

Where:

$\bar{X}$ = the mean conversion of the particles, [–]

$X(t)$ = function of conversion of a single particle over time t, [–]

In a CSTR, there is inflow and outflow of reactants and/or products. As a result, a mass balance for the continuous process can be written. The expression of X(t) in the "Reaction term" in the mass balance can change accordingly, as it depends on the chosen model used for the problem. This mass balance can be solved analytically with the simulation software (Matlab) and at a later stage, when more data are known, the code can be improved for higher accuracy, when transitioning from a batch mineralization process to a continuous one. The code "ScaleUp" is provided in Appendix B. Equation 2.16 is written in terms of accumulation for the case of conversion in a CSTR with the Shrinking Core Model, when chemical reaction is the controlling step. The derivation of Equation 2.16 is given in Appendix A.

$$\frac{dX}{dt} = \frac{3 * Mr_{Mg_2SiO_4} * R(T) * (1-X)^{\frac{2}{3}}}{r_p * \rho_p} + \frac{F_{olivine,in} * X_{initial} - F_{out} * \bar{X}}{V} \quad (2.16)$$

2.8 Gas-Liquid Mass Transfer Coefficient (k_La)

It was previously mentioned that the CO_2 dissolution rate is of great importance for the mineralization process and it could be the reason hindering the reaction. The k_La is interconnected with the gas-liquid mass transfer rate and is needed when designing the scale-up of a gas-liquid stirred tank reactor (STR) [36]. In order to reliably correlate k_La over a wide range of geometric configurations and operating parameters, an equation containing the relative dispersion term (N/N_{cd}), where N is the impeller speed [rev/s] and N_{cd} corresponds to the minimum impeller speed for complete dispersion of the sparged gas [rev/s] is frequently used [36]. Mixing at any impeller speed lower than N_{cd} leads to inefficient dispersion of the gas and thus, inefficient carbonation, because of the lack of CO_2. Based on the literature [36]:

$$k_La = 3.35 * \left(\frac{N}{N_{cd}}\right)^{1.464} * V_G \quad (2.17)$$

Where:

k_La = overall volumetric gas–liquid mass transfer coefficient, [s^{-1}]

V_G = superficial gas velocity, [m/s]

It must be noted that due to the early development of the pilot lab and the lack of measuring instruments of the CO_2 concentration in the gas and liquid phase and lack of mass flowmeter, Equation 2.17, which is usually used for industrial processes, could not be used. Nonetheless, Equation 2.17 could be used at a later stage of the process development to provide more accurate results.

Furthermore, another possible way of getting insight in regards to the k_La is through the pH of the solution. A linear relationship between pH and CO_2 solubility should exist though. An equation for this case in regards to CO_2 solubility in water has been proposed in the literature for different temperatures and pressures [46]:

$$pH = A * px + B \quad (2.18)$$

Where:

A, B = constants of the equation

$px = -\log(x)$, where x stands for the mole fraction of CO_2

Experiments of dilution in the system (CO_2 + H_2O) will be conducted to verify Equation 2.18. If verified, then some insight of the kLa can be gained by conducting experiments with pH measurements and by implementing Equation 2.19 [47]:

$$k_L a = 3.39 + 7.96 * T^* + 15.7 * Q^* + 18.8 * RPM^* + 6.46 * Q^{*^2} + 8.25 * T^* * Q^* \quad (2.19)$$

Where:

* = represents dimensionless terms

$T^* = \frac{T-27.5}{7.432}$ with T in °C

$Q^* = \frac{Q-1.1}{0.5351}$ with Q in L/min

$RPM^* = \frac{RPM-375}{133.8}$

The gas-liquid mass transfer in a continuous process can be formulated by the overall mass balance of CO_2 in the liquid phase of the slurry (mixture olivine and water). This is the following:

$$k_L a * \left(c^*_{CO_2} - \bar{c}_{CO_2}\right) * f_L * V_{SL} - \bar{R} * f_L * V_{SL} - F_{out} * f_L * \bar{c}_{CO_2} = 0 \quad (2.20)$$

Where:

k_L = mass transfer coefficient, [m/s]

a = specific interfacial area between gas and liquid phase, [m^2/m^3]

c_{CO_2} = concentration of dissolved CO_2 in the liquid phase, [mol/m^3]

$c^*_{CO_2}$ = concentration of CO_2 in the liquid phase at the gas-liquid interface of the bubbles under thermodynamic equilibrium with the gas phase, [mol/m^3]

$\bar{c}_{CO_2}$ = concentration of CO_2 in the bulk of the liquid phase of the slurry, [mol/m^3]

f_L = liquid fraction in the slurry, [m^3 liquid/m^3 slurry]

V_{SL} = volume of slurry in the reactor, [m^3]

$\bar{R}$ = average reaction rate of CO_2 to carbonate in the slurry, [$mol/m^3.s$]

F_{out} = volumetric flow rate of the product slurry at the outlet of the reactor, [m^3/s]

Equation 2.20 is characterized by 4 terms. The first one corresponds to the dissolving rate. Here, the driving force is the difference in concentrations of carbon dioxide between the liquid interfacial area and the bulk of the liquid. The second term represents the reaction of carbon dioxide to carbonate. The third term corresponds to the exit flow of dissolved CO_2 in the liquid phase of the outlet stream. Finally, the fourth term stands for the accumulation rate of dissolved CO_2 in the liquid phase of the slurry.

There are many experiments that can be performed at a later stage based on Equation 2.20 in order to simplify it and get an accurate result in regards to the gas-liquid mass transfer limitations under different process conditions and not only count on the k_La measurements, which cannot singlehandedly exclude these limitations.

3. Materials and Methods

3.1 Olivine

The olivine mineral used in this report was provided by GreenSand AB. The specific olivine material is characterized by a density of 3300 kg/m^3 and contains a small amount of Fe_2SiO_4, which also reacts with CO_2, but for the purpose of this project it is disregarded in the model implementation. More details for the material and information regarding the safety handling are provided in the safety sheet, which is presented in Appendix C.

The olivine material is presented below.

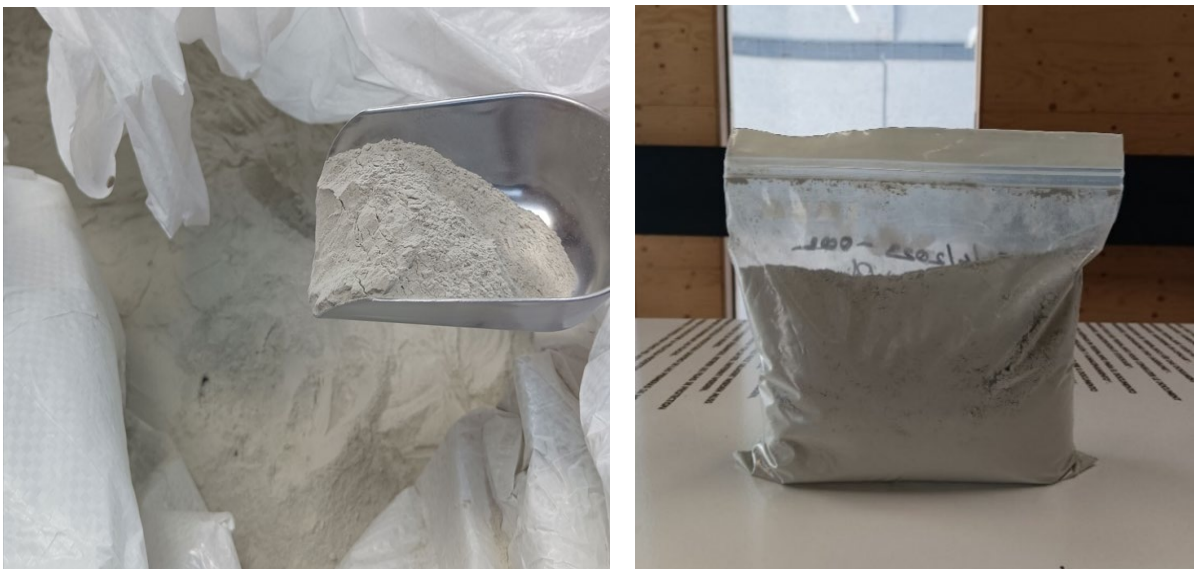

Figure 5. Collection and sampling of raw olivine (left) and reacted, dried olivine (right)

3.2 Experimental Setup and Procedure

Many types of reactors can be used for carbonation with different advantages and disadvantages. In this case, a high temperature batch autoclave reactor was used for conducting the experiments with different olivine particle sizes. In the case of the CO_2 dissolution experiments, a prototype plexiglass batch reactor was provided by Paebbl AB and operated under atmospheric pressure. The two reactors have similar dimensions so that the establishment of the basis in regards to the k_La measurements can be better approximated both during this and in future projects. The two reactors can be seen in Figure 6.

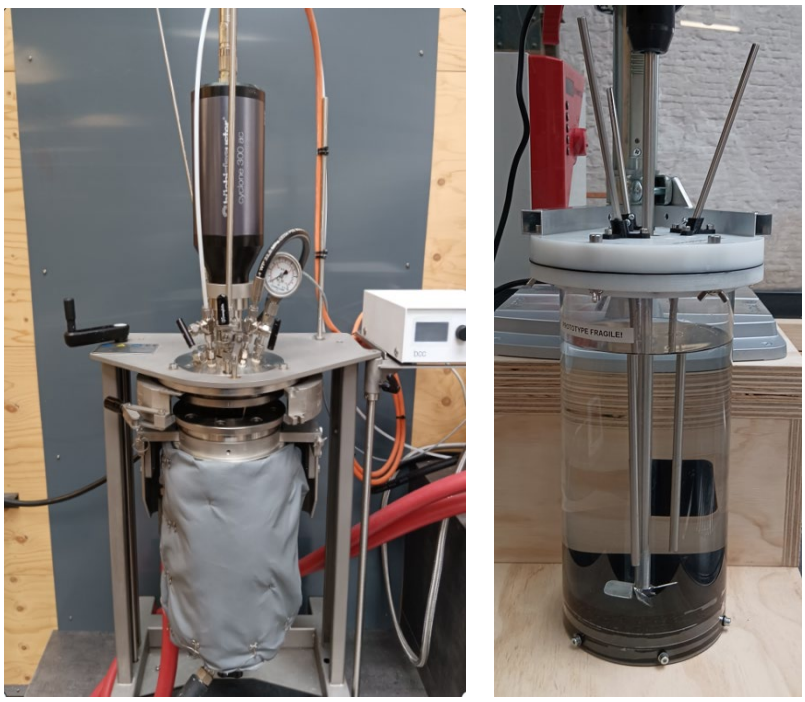

Figure 6. High temperature autoclave (left) and replica used for the mass transfer coefficient (k_La) estimations (right)

- High Temperature Autoclave Reactor

Based on reported data from the literature and the analysis presented above, the process of mineral carbonation of olivine with CO_2 should ideally be chosen to work under a pressure of 80 bar and temperature 175 ºC. This coincides with similar findings found the literature, where other setups were used [48]. Due to safety concerns, a lower pressure and temperature was chosen in this case (20 bar, 150 ºC respectively). Nonetheless, it must be noted that during the reaction the pressure reaches 40 – 50 bar depending on olivine particle size due to the

temperature increase in the reactor. The temperature affects the process more than the pressure. Higher pressures lead to shorter times required to reach a specific conversion. The reaction rate equation that was implemented in the simulation has temperature as the varying parameter and is derived through interpolation of pressure ranges from the literature.

The chemicals used in the high temperature autoclave are water (H_2O), sodium bicarbonate ($NaHCO_3$), oxalic acid dihydrate ($C_2H_2O_4 \bullet {}_2H_2O$), ascorbic acid ($C_6H_8O_6$) and a slurry mixture of olivine with water. In terms of the experimental procedure, the first step consists of the chemical mixture preparation. Olivine mixture is prepared by mixing approximately 470 gr of raw olivine with 170 gr of H_2O. The mixture is added into the reactor. Afterwards, 3.8 L of H_2O is poured into the autoclave chamber. 215 gr of $NaHCO_3$ are subsequently added gently in the chamber. Finally, 20 gr of oxalic acid dihydrate and 7 gr ascorbic acid are inserted into the reactor. The reactor is closed and sealed. A stirrer is connected to the reactor and before releasing CO_2 gas into the gas cap of the chamber at 20 bar, the stirring speed is set at 300 rpm. Subsequently, the cooling water feed is enabled and the temperature of the heating instrument (Unistat 405) is set at 150 ^oC. The pressure rises slowly inside the chamber due to the temperature increase and it can reach up to 45 – 50 bar depending on the particle size used. A sign that the reaction has started is the pressure drop observed, since the CO_2 concentration in the gas cap is decreasing, directly related to the CO_2 concentration in the solution through Henry's Law and the formation of product. The duration of the whole process is 3 h (approximately half an hour heating, 1 hour reaction and 1.5 hours cooling). The product mix can be seen in Figure 7.

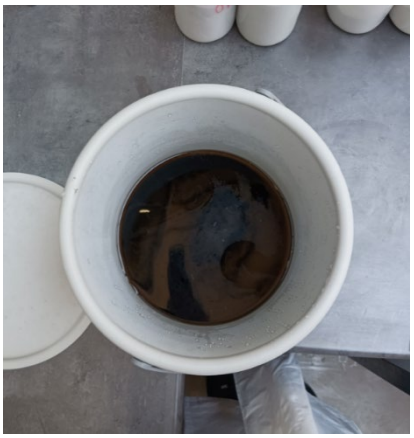

Figure 7. Collected product from the reactor before removing additives

Due to its weight, the product precipitates at the bottom. The dark-coloured liquid contains water and additives, which is then disposed. Afterwards, the product is inserted into a dryer overnight at 125 ^oC. This way most of the water that is left, evaporates.

Figure 8. End product before (left) and after drying (right)

The next step is the placing sample of the dried product in a furnace at 900 ºC for 2 hours. This way the Loss on Ignition (LOI) method can be utilized in order to calculate the conversion degree.

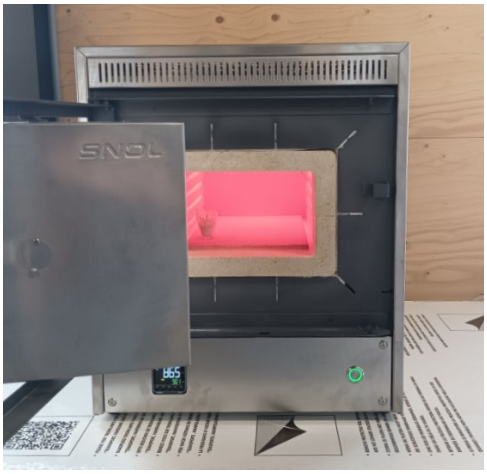

Figure 9. Furnace operated at 900 ºC for the LOI method

LOI is a common technique used for determining the percentage of combustible compounds present in a sample. High temperatures are required and the weight loss of the sample due to combustion of these compounds is measured. More specifically, if the product of mineralization ($MgCO_3$) undergoes Loss on Ignition, it is transformed into magnesium oxide (MgO) and CO_2 is also released. Nonetheless, it is important to mention that one limitation of this method is that non-volatile compounds can also be lost during the process. The olivine

contains also some very small quantities of crystal water, which can be released during the process.

It is important to highlight that at the time of the experiments, approval of operation for the high temperature autoclave was given, but not for commercial state due to safety concerns. The autoclave was operated at lower temperatures and pressures and due to this fact, the conversion of olivine was not the highest possible. Furthermore, due to a failure of the safety valve at the bottom of the high temperature autoclave reactor that led to a leak of CO_2, the experiments had to stop and not all of the olivine particle sizes were tested.4 runs were performed in total, two of which for reproducibility of results.

It is good to remember that the vessel operates at temperatures and pressures that exceed the ambient conditions by a lot. Although the raw material is not explosive or toxic, leaks from such a high temperature autoclave can possibly lead to explosion or damages and safety is always the first priority in such industrial processes, which is also stated in the Standard Operating Procedure manual (SOP).

- Plexiglass Reactor

The operating procedure in this case is much safer and simpler. At first, the reactor was filled in with tap water (~20 ^{o}C) at about the same height as the high temperature autoclave reactor. Afterwards, a pH-meter was inserted in the reactor and water inflow and outflow were enabled, reaching steady state. Subsequently, CO_2 at approximately 1 bar pressure was injected into the reactor and the stirring speed (initially set at 0) of a pitch-blade impeller was increased until bubbles of CO_2 (minimum dispersion) were formed in the liquid phase. It must be noted that although the system of (CO_2+H_2O) makes it easy to observe the formation of bubbles, but it still remains a visual determination, thus not 100% accurate. When bubbles started forming, minimum dispersion was achieved and the water outflow was collected in a beaker, while time measurements were also recorded to calculate the volumetric flow. The pH of the collected sample water was measured as soon as it was collected. The whole process was repeated with clean water between runs and with different volumetric flows and stirring speeds. Prior to these experiments, coarse olivine was injected into water and stirring speed was increased. A visual observation confirmed that the mixing approached ideal state.

3.3 Simulation Software

Matlab is a programming language and numerical computing environment that was developed by Mathworks. This software enables the user to solve numerically, simulate and even visualize results of complex systems. The reactor model in this dissertation was developed and simulated using the Matlab 2022a version [49].

For the current model, input parameters such as temperature, concentration and density of olivine are inserted into one file, which is named “Model”. This file executes the differential equation system solver (ODE function). The solver accuracy can be adjusted. The solver computes the result of the system of differential equations numerically in space and time and Figures of conversion versus time can be constructed. Additionally, another Matlab file was constructed containing the code for the scale-up of the process. This file is named “ScaleUp” and corresponds to the case of a continuous process with a 500L reactor. This code serves as a simulation example, where the effect of SCM resistances on conversion can be extrapolated to the case of a continuous process. For more information regarding the reaction model and the scale-up of the process in Matlab, please refer to Appendix B.

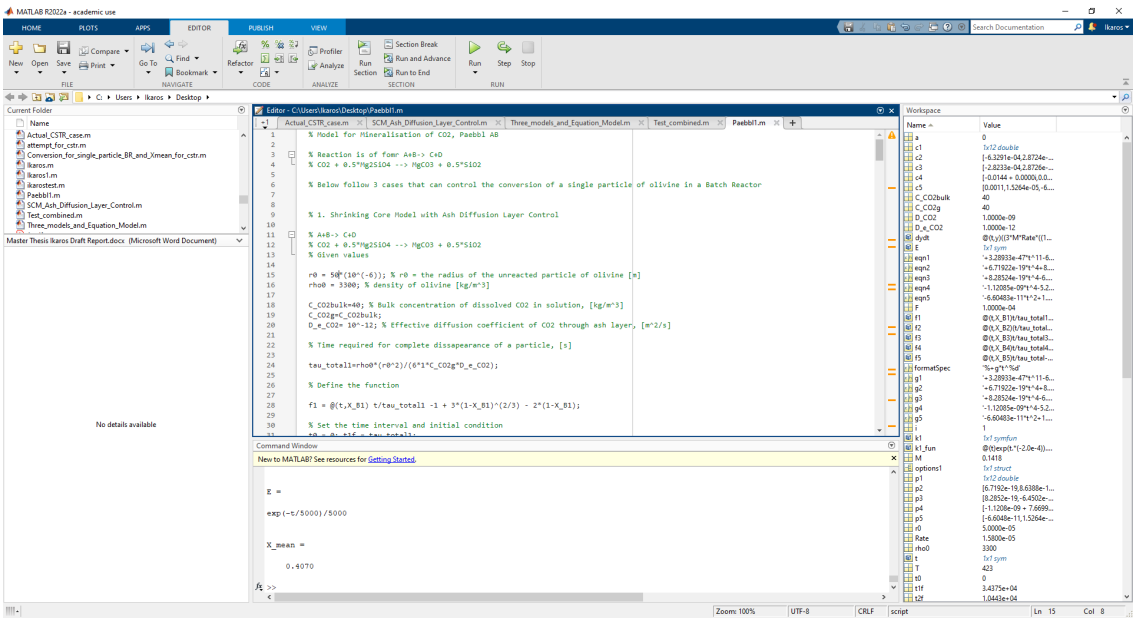

Figure 10. The interface of Matlab

4. Results and Discussion

Chapter 4 focuses on the presentation and discussion of the results of the project. Firstly, a comparison is made between the results of the simulation in regards to the effect of olivine particle size. Afterwards, the experimental data are compared to the developed model. Following this, insight is provided in regards to the findings regarding the CO_2 dissolution rate experiments. Finally, limitations of the project and potential areas for investigation are proposed.

4.1 Mineralization under different Olivine Particle Sizes

As mentioned before, the three resistances that can potentially play a role in the process are Product Layer Diffusion Resistance, Reaction Rate Resistance and Film Diffusion Resistance. Each one of those was modelled for 4 cases of pure olivine particles with the following radius:

- 10 um
- 20 um
- 50 um
- 100 um

It should be mentioned here, that raw olivine material with 100um particle size is considered coarse and is not actively being used in the process developed by Paebbl AB. For a better visual understanding of the process, Paebbl AB provided pictures of the raw and carbonated material, both of which can be seen in Figure 11 below.

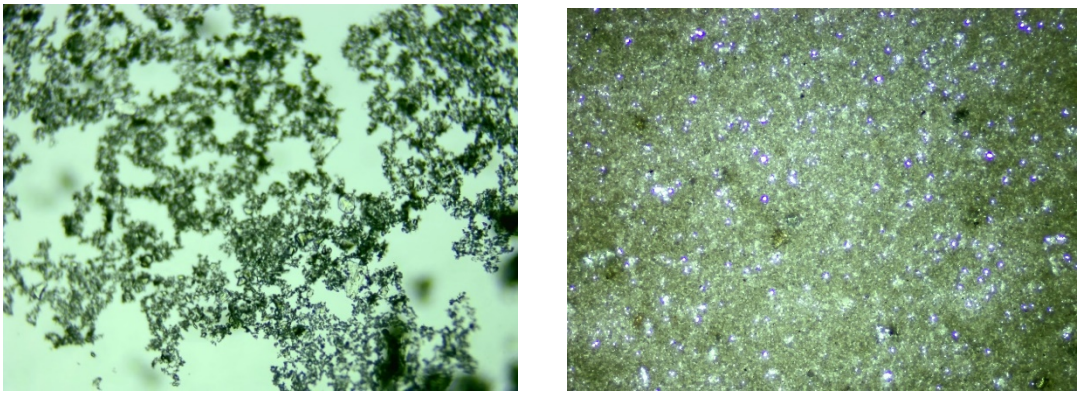

Figure 11. Raw olivine (left) and mineralized CO_2 with olivine under the microscope – grey spots (right) [Courtesy of Paebbl AB]

In Figure 12, the results regarding the Product Layer Diffusion resistance are presented.

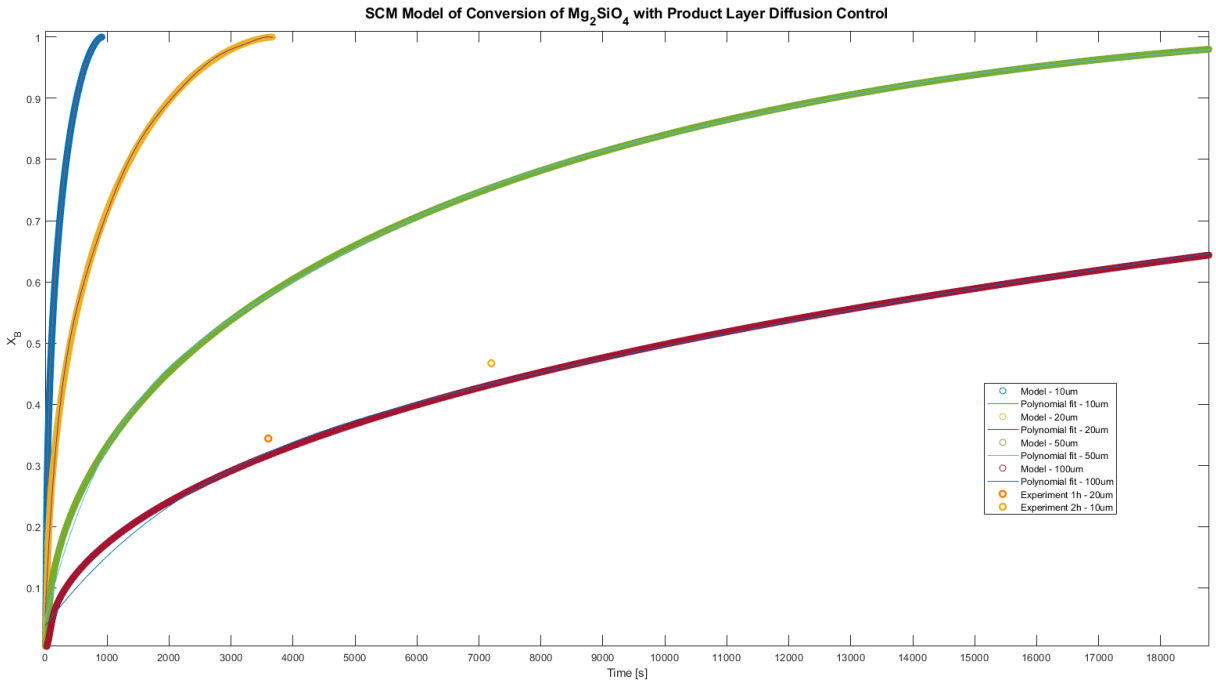

Figure 12. Effect of particle size on the conversion of olivine under Product Layer Diffusion resistance

It is apparent that olivine particle size greatly affects the time required for total conversion. Just by increasing the olivine particle size by 100% (10um to 20um), the time required for total conversion is increased by approximately 4 times. This effect becomes even stronger when addressing larger particles. Taking into comparison 10um and 50um particles, it can be seen that the total time for conversion is increased by about 21 times. This can be explained, simply by the fact that as CO_2 reacts with the olivine, product is formed around the unreacted core. The bigger the particle, the thicker this product layer becomes, thus making it harder for CO_2 to reach the unreacted core, through the means of the diffusion coefficient.

The orange and yellow points represent the experimental result of 20um particles (1h process) and 10um particles (2h process), respectively. Based on the results, it is quite evident that the experimental and modelling results for both particle sizes (represented by the blue and yellow lines) are vastly different. The 20um particle reached only 34.4% conversion after a 1 hour process, whereas, based on the model, conversion is rapid and should be equal to 100% for the same time. Similarly, for the 10um particles, conversion reached only 46.7% after 2 hours. This type of resistance cannot be proposed as the governing mechanism of the process. Interestingly enough though, the experimental results follow the pattern of the modelled curve

for the case of 100um particles, although a comparison cannot be made at this point. Reasons that might be responsible for the presented differences will be discussed in the conclusions.

When the Chemical Reaction is considered the resistance, a similar trend is followed.

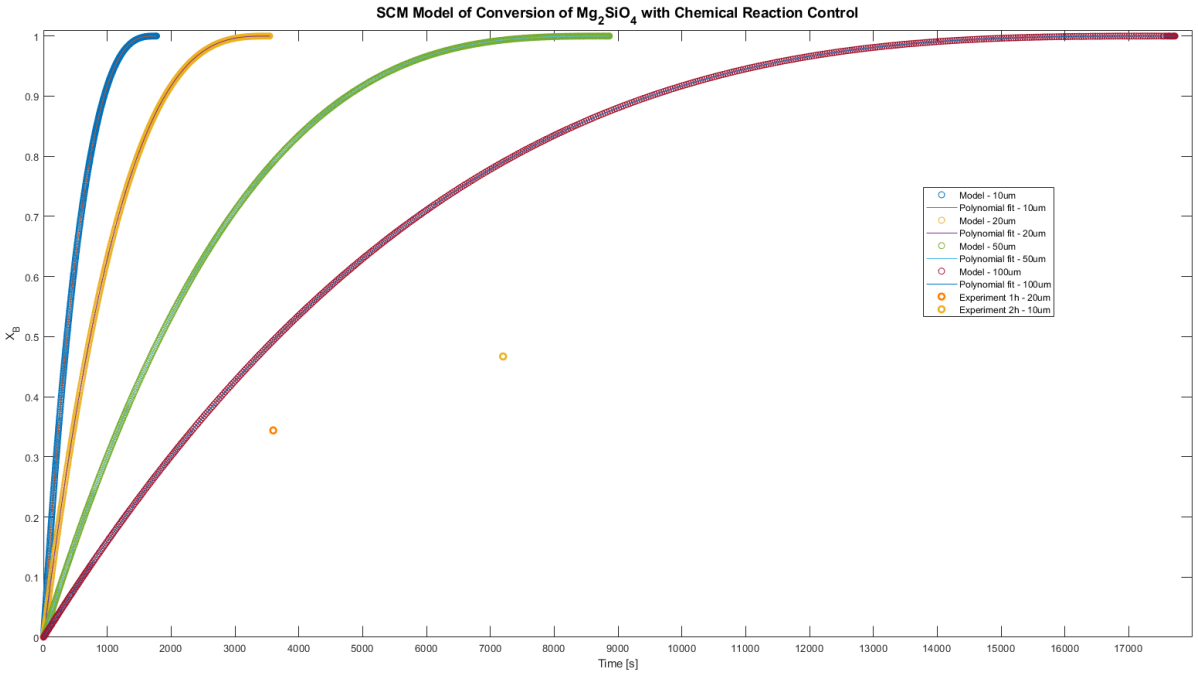

Figure 13. Effect of particle size on the conversion of olivine under Chemical Reaction resistance

Just like in the case of Product Layer Diffusion resistance, the greater the particle size, the longer the time required for full conversion of a particle becomes. The differences though in this case are first of all, that the time required for full conversion of an olivine particle and particle size are proportional. For example, a 10um olivine particle needs approximately 0.5 hours to reach 100% conversion, whereas 20um and 100um particles need 1 hour and 5 hours, respectively. This is also apparent by the literature equations of the model, which are included in the Matlab code. The second finding is interesting and regards the time required for total conversion. When compared to the Product Layer Diffusion resistance case of a particle of the same size, it is evident that in this case a 10um olivine particle will require approximately 43% more time to react completely. As the particle size is increased this relationship starts to favour the Chemical Reaction resistance. Based on the Model, a 20um particle will require approximately the same time (1 hour) for 100% conversion in these two cases, whereas bigger particles need less time for full conversion, when Chemical Reaction is the controlling step in the process. Another interesting takeaway is the fact that when the Product Layer Diffusion is the controlling step, at the beginning of the process fast conversion can be achieved, at least

theoretically. This will also be further discussed in the conclusions. When it comes to the experimental results, it is apparent from Figure 13 that the experimental and modelling results are once again greatly different.

The final resistance that was modelled considers the case of the Film Diffusion Control, meaning that the liquid film around the particle, accompanied by steep concentration gradients of CO_2 gas within that, is the limiting step. Due to the form of the literature equations, the modelled case here results in linear lines. In this case, when implementing the model, the bulk concentration of dissolved CO_2 in the solution is required. The required input was provided by Paebbl AB and inserted in the Matlab code, while also taking into account the assumption that there is no transfer resistance for CO_2 present in the gas-liquid interface of the solution as previously mentioned (Table 1), due to higher diffusivity in the gas phase.

In general, when compared to the other models, this case presents the fastest times, when it comes to time required for total conversion of the particles. Furthermore, the time required for full conversion presents a proportional relationship with particle size as in the case of Chemical Reaction resistance. Nonetheless, this third case cannot singlehandedly describe the experimental process, as can be seen by the in Figure 14 below.

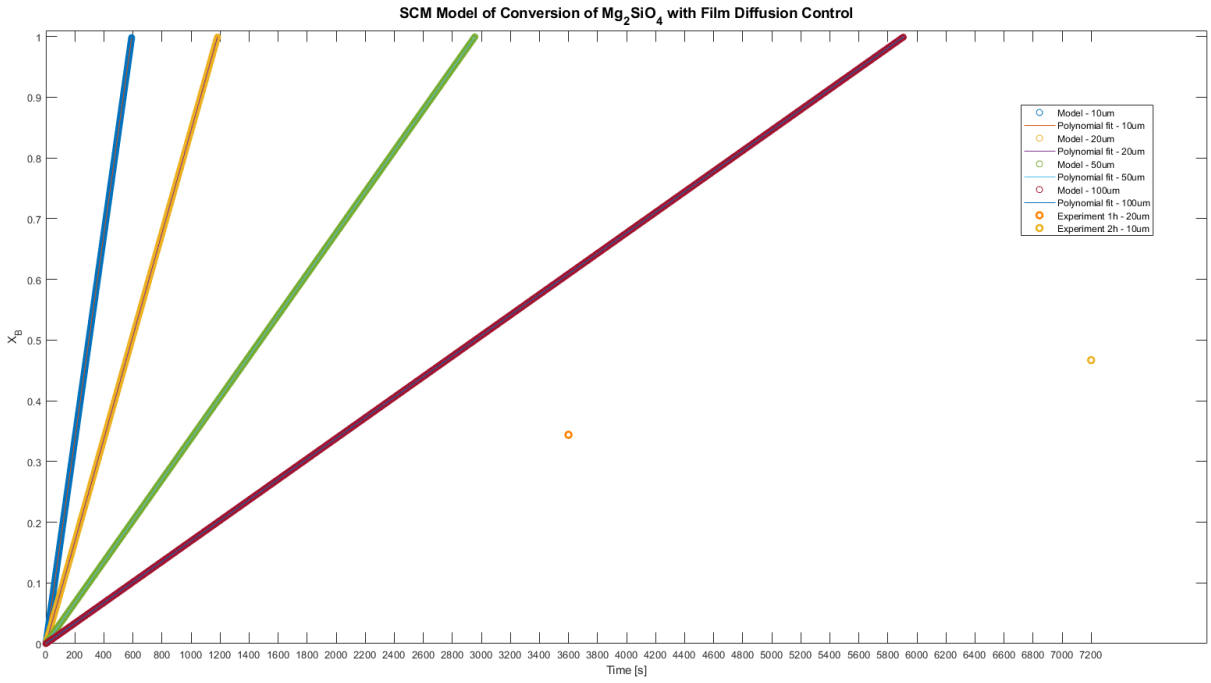

Figure 14. Effect of particle size on the conversion of olivine under Film Diffusion resistance

4.2 CO_2 Dissolution Rate (k_La)

As stated before, an initial estimation of the CO_2 dissolution rate and determination whether or not it is a limiting factor in the process can be made through the overall mass transfer coefficient (k_La). At this stage, experiments were conducted with CO_2 and water in the plexiglass reactor. This is partly because of lack of available instruments for more accurate and complex experiments and due to the fact that some basic understanding has to be acquired by laying the foundation of experimentation before moving to more complex problems. Nonetheless, the system of CO_2 and water gives a rough initial idea in regards to the possible mass transfer limitations.

The plexiglass reactor has similar dimensions to the high temperature autoclave reactor in order to provide a better approximation of the k_La through experimentation. This reactor was chosen as a suitable solution for experimentation also due to the nature of the process (high pressure and temperature), which would not be possible in the high temperature autoclave.

Based on literature data, there is a linear relationship between pH and CO_2 dissolution in water [46], described by Equation 2.18:

$$pH = A * (px) + B$$

This linear correlation was verified in this case, as can be seen in Figure 15 below.

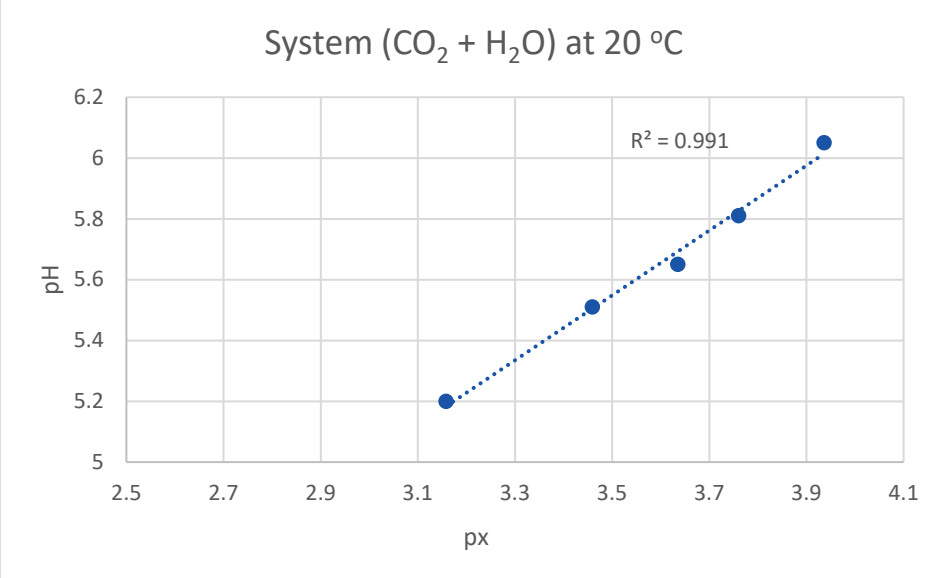

Figure 15. Correlation of pH and solubility of CO_2 (mol/kg) in water at 20 °C

With this linear correlation verified, the quick reduction of pH of water during experimentation can be beneficial for acquiring some insight in regards to the k_La. The faster the drop of pH in solution, the faster the dissolution of CO_2 becomes.

Equation 2.19 can be utilized to get an estimate of the k_La in every experimental case, thus making it possible to calculate the average k_La. Computed values should not be taken as fully applicable in the real-life case scenario of the process. Although Equation 2.19 was derived based on same type of impeller as the one inside the plexiglass reactor, the dimensions of the reactor described in the literature were smaller and it is known that properties of the system affect the k_La measurements. Nonetheless, utilizing Equation 2.19 still holds value, since some insight can be gained regarding k_La. An example of calculation is presented below. The same procedure was followed for the other calculations based on the values presented in Table 2.

Table 2. Parameters required for determination of average k_La

Experiment No.	Stirring Speed (RPM)	Volumetric Flowrate (mL/sec)	pH	T (ºC)
1	1650	74	5.90	20
2	1340	45	5.53	20
3	1250	23	5.32	20
4	980	7	5.30	20
5	1150	72	5.91	20
6	1360	7.5	5.32	20

For the case of Experiment 1:

$$k_La = 3.39 + 7.96 * T^* + 15.7 * Q^* + 18.8 * RPM^* + 6.46 * Q^{*^2} + 8.25 * T^* * Q^* \rightarrow$$

$$k_La = 3.39 + 7.96 * \left(\frac{20-27.5}{7.432}\right) + 15.7 * \left(\frac{74*\frac{60}{1000}-1.1}{0.5351}\right) + 18.8 * \left(\frac{1650-375}{133.8}\right) + 6.46 *$$

$$\left(\frac{74*\frac{60}{1000}-1.1}{0.5351}\right)^2 + 8.25 * \left(\frac{20-27.5}{7.432}\right) * \left(\frac{74*\frac{60}{1000}-1.1}{0.5351}\right) \rightarrow$$

$$k_La = 335\ h^{-1}$$

Table 3. Dimensionless parameters required for determination of average k_La

Experiment No.	T*	Q*	RPM*	Q^{*2}	T*Q*	Estimated k_La (h^{-1}, Eq. 2.19)
1	-1.01	4.44	9.53	19.7	-4.48	335
2	-1.01	2.7	7.21	7.29	-2.72	198
3	-1.01	1.38	6.54	1.90	-1.39	141
4	-1.01	0.42	4.52	0.176	-0.423	84.5
5	-1.01	4.32	5.79	18.7	-4.36	257
6	-1.01	0.45	7.36	0.203	-0.454	138

The mean value of k_La for our system is equal to 192 h^{-1}. This value is lower than the k_La reported for diffusion of O_2, which has been reported to reach even up to 200 h^{-1} at lower stirring rates. This makes sense, since the diffusion coefficient of O_2 is higher than that of CO_2 in water [47]. It must be noted that Equation 2.19, which was used for obtaining these results, gives a good approximation at stirring rates up to 600 RPM, but it was assumed that the accuracy level was not affected above that, partly due to the lack of literature data to support otherwise. An interesting finding is that the greatest change in pH occurs between the highest (Experiment 1) and lowest (Experiment 4) stirring rates and flowrates. This change in pH is still small and within the margins of experimental error. Thus, in all cases the stirring speeds and flowrates were proved to be adequate in regards to the transfer of CO_2 from the gas to the liquid phase and almost equally efficient, as proven by the low pH values of the water outflows. Furthermore, Experiments 5 and 6 provide similar results as Experiments 1 and 4, respectively, suggesting that the flowrate has a greater impact in the mass transfer, with lower stirring rates being adequate for CO_2 to get sucked into the liquid phase. It must be noted that the observations of this phenomenon were visual, thus adding greater risk for error. The effect of lower stirring rates could not be investigated, due to the lack of instrumentation.

With the current data and results available, the k_La value cannot be considered small enough, so that CO_2 dissolution becomes the limiting factor for the process. Better experimental design with proper instrumentation, such as mass flowmeters and submerged CO_2 sensors in liquids, can be implemented in the future to get a better understanding and more accurate and concrete results should be derived by utilizing the overall mass balance presented in Chapter 2.8 (Equation 2.20), since from k_La alone it cannot be directly concluded that the gas-liquid mass transfer is not limiting. This way it can be validated that at different process rates the concentration at the bulk remains close to the interface concentration. Furthermore, experimental design accounting for the same slurry mixture used in the high temperature autoclave should be developed.

5. Conclusions

In conclusion, several limitations are identified through this project, as will be discussed below, but also important insight is gained. In regards to the effect of the olivine particle size in mineralization, it was observed that increasing the particle size, significantly increased the time required for total conversion regardless of the resistance type. The modelled resistances cannot describe the process accurately, thus hinting towards a uniform effect of all three of them on mineralization of olivine simultaneously. The rapid conversion in the case of the Product Layer Diffusion control could also be due to a possibly smaller diffusion coefficient than the one implemented in the model based on the available literature. Reaction rate and film diffusion resistances might be more evident in the beginning of the process, when a small or no product layer exists around the unreacted core. Resistance from the product layer can become significant as the product layer grows. Nonetheless, it should be noted that more data must be acquired to better understand the process and limitations, such as the porosity of the material, the actual impurities and their effect on conversion limitation, but also the effect of the by-product silica (SiO_2), which exists on the product layer, in cavities and pores and which is most likely also hindering the process.

When it comes to the experimental results, mineralizing 20um particles under 1 hour led to 34.4% conversion, whereas mineralizing 10um particles under 2 hours led to a conversion of 46.7%. Although this is an increase of about 12% in terms of conversion, a thorough investigation of energy requirements (such as milling energy input) should be conducted in the future to assess whether or not smaller particles sizes is a sustainable and economically viable choice. Furthermore, due to time limitations, experimental delays and safety concerns it is suggested for future projects more experiments to be conducted with different particles sizes and under longer process times in order to get a better idea of the process.

Experiments with CO_2 and water in a plexiglass reactor provided initial insights into the mass transfer limitations. These experiments in regards to the possible CO_2 dissolution rate limitation for the process, through the overall mass transfer coefficient (k_La), suggest that the k_La is not small enough to make CO_2 dissolution the limiting factor in the process. The results indicated that the stirring speed and flowrate were adequate for efficient transfer of CO_2 from the gas to the liquid phase with the calculated average k_La value being equal to 192 h^{-1}, which is lower than that reported for O_2. Due to the lack of instrumentation, the impact of lower stirring rates could not be fully explored. Future research should aim to address these limitations, explore other improved experimental designs, while also utilizing the Equations presented in this report and a (CO_2 + olivine) system.

6. Bibliography

1. Reichle, D.E., (2020). Anthropogenic alterations to the global carbon cycle and climate change. *The Global Carbon Cycle and Climate Change*. Elsevier, pp. 209–251. https://doi.org/10.1016/B978-0-12-820244-9.00011-1

2. Ganopolski, A., (2008). Climate Change Models. *Encyclopedia of Ecology*. Elsevier, pp. 603–612. https://doi.org/10.1016/B978-008045405-4.00197-X

3. Solomon, S., Plattner, G.-K., Knutti, R., Friedlingstein, P., (2009). Irreversible climate change due to carbon dioxide emissions. *Proc. Natl. Acad. Sci. U.S.A.*, 106, pp. 1704–1709. https://doi.org/10.1073/pnas.0812721106

4. United Nations Treaty Collection. (2016). Paris Agreement. Retrieved from https://treaties.un.org/doc/Treaties/2016/02/20160215%2006-03%20PM/Ch_XXVII-7-d.pdf

5. European Commission. European Green Deal. (2020). Retrieved from https://commission.europa.eu/strategy-and-policy/priorities-2019-2024/european-green-deal_en

6. Cuéllar-Franca and R.M., Azapagic, A., (2015). Carbon capture, storage and utilisation technologies: A critical analysis and comparison of their life cycle environmental impacts. *Journal of CO_2 Utilization*, 9, pp. 82–102. https://doi.org/10.1016/j.jcou.2014.12.001

7. Abdulla, A., Hanna, R., Schell, K.R., Babacan, O., Victor, D.G., (2021). Explaining successful and failed investments in U.S. carbon capture and storage using empirical and expert assessments. *Environ. Res. Lett.*, 16, 014036. https://doi.org/10.1088/1748-9326/abd19e

8. Bui, M., et al., (2018). Carbon capture and storage (CCS): the way forward. *Energy Environ. Sci.*, 11, pp. 1062–1176. https://doi.org/10.1039/C7EE02342A

9. Satter, A. and Iqbal, G.M., (2016). Enhanced oil recovery processes: thermal, chemical, and miscible floods. *Reservoir Engineering*. Elsevier, pp. 313–337. https://doi.org/10.1016/B978-0-12-800219-3.00017-6

10. Vishal, V. and Singh, T.N. (Eds.), (2016). Geologic Carbon Sequestration. Springer International Publishing, Cham., pp. 249-284. https://doi.org/10.1007/978-3-319-27019-7

11. Peres, C.B., Resende, P.M.R., Nunes, L.J.R., Morais, L.C.D., (2022). Advances in Carbon Capture and Use (CCU) Technologies: A Comprehensive Review and CO_2 Mitigation Potential Analysis. *Clean Technol.*, 4, pp. 1193–1207. https://doi.org/10.3390/cleantechnol4040073
12. Dibenedetto, A., Angelini, A., Stufano, P., (2014). Use of carbon dioxide as feedstock for chemicals and fuels: homogeneous and heterogeneous catalysis: Use of carbon dioxide as feedstock for chemicals and fuels. *J. Chem. Technol. Biotechnol.*, 89, pp. 334–353. https://doi.org/10.1002/jctb.4229

13. Jiang, K. and Ashworth, P., (2021). The development of Carbon Capture Utilization and Storage (CCUS) research in China: A bibliometric perspective. *Renewable and Sustainable Energy Reviews*, 138, 110521. https://doi.org/10.1016/j.rser.2020.110521

14. Razzak, S.A., Ali, S.A.M., Hossain, M.M., deLasa, H., (2017). Biological CO_2 fixation with production of microalgae in wastewater – A review. *Renewable and Sustainable Energy Reviews*, 76, pp. 379–390. https://doi.org/10.1016/j.rser.2017.02.038

15. Kougias, P.G., et al., (2020). Biological CO_2 fixation in up-flow reactors via exogenous H_2 addition. *Journal of Biotechnology*, 319, pp. 1–7. https://doi.org/10.1016/j.jbiotec.2020.05.012

16. Gadikota, G., (2021). Carbon mineralization pathways for carbon capture, storage and utilization. *Commun Chem*, 4, pp. 23. https://doi.org/10.1038/s42004-021-00461-x

17. Armstrong, K., (2015). Emerging Industrial Applications. *Carbon Dioxide Utilisation*. Elsevier, pp. 237–251. https://doi.org/10.1016/B978-0-444-62746-9.00013-X

18. Hills, C.D., Tripathi, N., Carey, P.J., (2020). Mineralization Technology for Carbon Capture, Utilization, and Storage. *Front. Energy Res.*, 8. https://doi.org/10.3389/fenrg.2020.00142

19. Zevenhoven, R. and Kavaliauskaite, I., (2004). Mineral carbonation for long-term CO_2 storage: an exergy analysis. *International Journal of Thermodynamics*, 7 (1), pp. 23-31.

20. Skocek, J., Zajac, M., Ben Haha, M., (2020). Carbon Capture and Utilization by mineralization of cement pastes derived from recycled concrete. *Sci Rep*, 10, 5614. https://doi.org/10.1038/s41598-020-62503-z

21. Rafferty, J.P. (Ed.). (2011). Minerals. Geology: Landforms, Minerals, and Rocks Series. Rosen Publishing Group, ISBN 978-1615304899

22. Miller, B.G., (2011). CO_2 Capture and Storage, *Clean Coal Engineering Technology*. Elsevier, pp. 483–511. https://doi.org/10.1016/B978-1-85617-710-8.00010-8

23. Reay, D., Ramshaw, C., Harvey, A., (2013). Application Areas – Petrochemicals and Fine Chemicals, *Process Intensification*. Elsevier, pp. 259–321. https://doi.org/10.1016/B978-0-08-098304-2.00008-0

24. Klein, C. (1998). Manual of Mineralogy (after James D. Dana), 21st Edition, Revised. Wiley.

25. Oelkers, E.H., Gislason, S.R., Matter, J., (2008). Mineral Carbonation of CO_2. *Elements*, 4, pp. 333–337. https://doi.org/10.2113/gselements.4.5.333

26. National Academies of Sciences, Engineering, and Medicine. (2019). Negative Emissions Technologies and Reliable Sequestration: A Research Agenda. Washington, DC: The National Academies Press (US). https://doi.org/10.17226/25259

27. Schuiling, R.D. and Krijgsman, P. (2006). Enhanced weathering: An effective and cheap tool to sequester CO_2. *Climatic Change*, 74, pp. 349-354. https://doi.org/10.1007/s10584-005-3485-y

28. Wang, F., Dreisinger, D., Jarvis, M., Hitchins, T., (2019). Kinetics and mechanism of mineral carbonation of olivine for CO_2 sequestration. *Minerals Engineering*, 131, pp. 185–197. https://doi.org/10.1016/j.mineng.2018.11.024

29. Matus, C., et al. (2020). Mechanism of Nickel, Magnesium, and Iron Recovery from Olivine Bearing Ore during Leaching with Hydrochloric Acid Including a Carbonation Pre-Treatment. *Metals*, 10, 811. https://doi.org/10.3390/met10060811

30. Huijgen, W.J.J., Witkamp, G.-J., Comans, R.N.J., (2006). Mechanisms of aqueous wollastonite carbonation as a possible CO_2 sequestration process. *Chemical Engineering Science*, 61, pp. 4242–4251. https://doi.org/10.1016/j.ces.2006.01.048

31. Senanayake, G., (2007). Review of theory and practice of measuring proton activity and pH in concentrated chloride solutions and application to oxide leaching. *Minerals Engineering*, 20, pp. 634–645. https://doi.org/10.1016/j.mineng.2007.01.002

32. Saran, R.K., Arora, V. and Yadav, S., (2018). CO_2 Sequestration by Mineral Carbonation: A Review. *Global NEST Journal*, 20, pp. 497–503. https://doi.org/10.30955/gnj.002597

33. Verbeeck W. (2012). Sustainable Carbon Dioxide Sequestration Using Integrated Mineral Carbonation Reactor Technology. Master's Thesis, KU Leuven

34. Tai, C.Y., Chen, W.-R. and Shih, S.-M., (2006). Factors affecting wollastonite carbonation under CO_2 supercritical conditions. *AIChE Journal*, 52, pp. 292–299. https://doi.org/10.1002/aic.10572

35. Henry's Law, An extensive list of Henry's law constants, and a conversion tool. www.henrys-law.org, (19/02/2023)

36. Yawalkar, A.A., Heesink, A.B.M., Versteeg, G.F., Pangarkar, V.G., (2008). Gas-Liquid Mass Transfer Coefficient in Stirred Tank Reactors. *Can. J. Chem. Eng*, 80, pp. 840–848. https://doi.org/10.1002/cjce.5450800507

37. Green, D.W. and Perry, R.H. (1984). Perry's Chemical Engineers' Handbook, 6th Edition. McGraw-Hill. ISBN 0-07-049479-7

38. Sander, R., Acree, W.E., De Visscher, A., Schwartz, S.E., Wallington, T.J., (2022). Henry's law constants (IUPAC Recommendations 2021). *Pure and Applied Chemistry*, 94, pp. 71–85. https://doi.org/10.1515/pac-2020-0302

39. Haug, A. (2010). Dissolution and carbonation of mechanically activated olivine. Doctoral dissertation, University of Trondheim.

40. Lackner, K.S., Wendt, C.H., Butt, D.P., Joyce, E.L., Sharp, D.H., (1995). Carbon dioxide disposal in carbonate minerals. *Energy*, 20, pp. 1153–1170. https://doi.org/10.1016/0360-5442(95)00071-N

41. Lackner, K.S., (2002). Carbonate Chemistry for Sequestering Fossil Carbon. *Annu. Rev. Energy. Environ.*, 27, pp. 193–232. https://doi.org/10.1146/annurev.energy.27.122001.083433

42. Pokrovsky, O. S., and J. Schott. (2004). Experimental study of brucite dissolution and precipitation in aqueous solutions: Surface speciation and chemical affinity control. *Geochimica Et Cosmochimica Acta*, 68(1), pp. 31-45. https://doi.org/10.1016/S0016-7037(03)00238-2

43. Levenspiel, O. (1998). Chemical reaction engineering, 3rd Edition. John Wiley & Sons. ISBN: 978-0-471-25424-9.

44. Fogler, H. S. (2016). Elements of chemical reaction engineering, 5th Edition. Pearson. ISBN: 978-0133887518

45. Viitanen, P., (2005). RADIOCHEMICAL METHODS: Radiotracers. *Encyclopedia of Analytical Science*. Elsevier, pp. 50–58. https://doi.org/10.1016/B0-12-369397-7/00522-7

46. Mohammadian, E. et al. (2023). Probing Solubility and pH of CO2 in aqueous solutions: Implications for CO2 injection into oceans, *Journal of CO2 utilization*, 71, pp. 102463. https://doi.org/10.1016/j.jcou.2023.102463

47. Hill, G. A. (2006). Measurement of overall volumetric mass transfer coefficients for carbon dioxide in a well-mixed reactor using a pH probe. *Industrial & engineering chemistry research*, 45 (16), pp. 5796–5800. https://doi.org/10.1021/ie060242t

48. Wang, F., Dreisinger, D., Jarvis, M., Hitchins, T., Dyson, D., (2019). Quantifying kinetics of mineralization of carbon dioxide by olivine under moderate conditions. *Chemical Engineering Journal*. 360, pp. 452–463. https://doi.org/10.1016/j.cej.2018.11.200

49. The MathWorks Inc. (2022). MATLAB version: 9.12.0.2039608 (R2022a), Natick, Massachusetts: The MathWorks Inc. https://www.mathworks.com

Appendix A – SCM Scale Up

The analytical calculations for the shrinking core model with chemical reaction control are presented in this section. The governing equations for the case of the shrinking particle model that were used in the simulation are also included. Appendix A comprises additionally of the mass balance in regards to the case of the CSTR.

Reactor balance for Batch reactor, Constant Volume applied on SCM with Chemical Reaction Control

The general mass balance equation can be written generally as "Accumulation = In – Out + Generation". More specific though, by taking into account the conservation of mass, the material balance for a batch reactor can be written as:

$$\frac{d}{dt}\int_V c_i\, dV = F_{in} * c_{i,in} - F_{out} * c_{i,out} + \int_V R_i\, dV \quad (A1)$$

Where:

F = volumetric flow rate, $\left[\frac{m^3}{sec}\right]$

i = every component present in the reactor, including inerts that do not take part in any reaction

c = concentration of reactant, $\left[\frac{mol}{m^3}\right]$

R = reaction rate (units depend on order of reaction)

V = volume of reactor, $[m^3]$

Assuming that the batch reactor is well-stirred and that the entire reactor is the reactor volume and taking into account that in a batch reactor there is no inflow or outflow ($F_{in} = F_{out} = 0$), Equation A1 can be transformed into:

$$\frac{d(c_i * V)}{dt} = R_i * V \quad (A2)$$

For constant reactor volume or if the volume of the reactor does not change significantly during operation, Equation A2 is simplified to:

$$\frac{dc_i}{dt} = R_i \ (A3)$$

The shrinking core model with constant particle size with chemical reaction control was chosen. In this case, the modified reaction rate is proportional to the surface of the unreacted core of the particle.

The reaction of interest is:

$$CO_2 + \frac{1}{2}\, Mg_2SiO_4 \rightarrow MgCO_3 + \frac{1}{2}\, SiO_2$$

$$A_{(g)} + bB_{(s)} \rightarrow solid\ products$$

Where:

A = CO_2, B = Mg_2SiO_4, C = $MgCO_3$ and D = SiO_2

Reaction rewritten with 1 mol of Mg_2SiO_4 as base of calculations:

$$2CO_2 + Mg_2SiO_4 \rightarrow 2MgCO_3 + SiO_2$$

As previously mentioned, the rate is directly proportional to the available surface of unreacted core disregarding any ash layer (product).

$$-2\frac{dN_A}{dt} = -\frac{dN_B}{dt} = R(T) * A(r_c) \quad (A4)$$

Where:

r_c = the radius of the unreacted core, $[m]$

$A(r_c)$ = surface area of unreacted core, $[m^2]$

We know as well from Levenspiel [43], that for this case:

$$\frac{t}{\tau} = 1 - \frac{r_c}{r_p} = 1 - (1 - X_B)^{1/3} \rightarrow \frac{r_c}{r_p} = (1 - X_B)^{1/3} \rightarrow \left(\frac{r_c}{r_p}\right)^3 = 1 - X_B \quad (A5)$$

Where X_B is the conversion of the particle [-] and r_p is the radius of the unreacted particle [m].

The total moles (N_{tot}) in an unreacted particle and the remaining number of unreacted moles in a particle (N) are correlated by the following equation:

$$N = N_{tot} * (1 - X_B)\ [moles] \quad (A6)$$

Furthermore, the particles are considered spherical:

$$V_p = \frac{4 * \pi * {r_p}^3}{3} \quad (A7)$$

$$\rho_p = \frac{m_p}{V_p} = \frac{N_{tot} * Mr_p}{V_p} = \frac{N_{tot} * Mr_{Mg_2SiO_4} + \sum_{i=0}^{n} N_{impurity,i} * Mr_{impurity,i}}{V_p} \quad (A8)$$

Where V_p is the volume of a spherical particle $[m^3]$, ρ_p is the density of the spherical particle $(\frac{kg}{m^3})$, $Mr_{Mg_2SiO_4}$ is equal to the molar mass of magnesium silicate $(\frac{kg}{mol})$ and i every component that acts as an impurity.

It must be noted that at this point and given the scope of the thesis and the limited data, the term of impurities can be neglected $(\sum_{i=0}^{n} N_{impurity,i} * Mr_{impurity,i} = 0)$ and is assumed that the liquid phase is saturated with CO_2.

As a result, by combining Equations A7 & A8:

$$N_{tot} = \frac{4 * \pi * {r_p}^3 * \rho_p}{3 * Mr_{Mg_2SiO_4}} \quad (A9)$$

Additionally, based on Equation A5:

$$A(r_c) = 4 * \pi * {r_c}^2 = 4 * \pi * {r_p}^2 * (1 - X_B)^{\frac{2}{3}} \quad (A10)$$

Afterwards Equation A9 is substituted into Equation A6:

$$N = N_{tot} * (1 - X_B) = \frac{4 * \pi * {r_p}^3 * \rho_p}{3 * Mr_{Mg_2SiO_4}} * (1 - X_B) \quad (A11)$$

By substituting Equation A10 into Equation A4:

$$-\frac{dN}{dt} = R(T) * A(r_c) = R(T) * 4 * \pi * {r_p}^2 * (1 - X_B)^{\frac{2}{3}} \quad (A12)$$

Conversion X, for example for magnesium silicate (Mg_2SiO_4), can be written as:

$$X = \frac{N_{initial} - N_{final}}{N_{initial}} = \frac{N_{total} - N}{N_{total}} \quad (A13)$$

Using Equations A4, A6, A9 & A13:

$$\frac{dN}{dt} = \frac{d(N_{tot}*(1-X_B))}{dt} = -N_{tot} * \frac{dX}{dt} \rightarrow -\frac{dN}{dt} = \frac{4*\pi*{r_p}^3*\rho_p}{3*Mr_{Mg_2SiO_4}} * \frac{dX}{dt} \quad (A14)$$

By combining Equations A12 & A14:

$$-\frac{dN}{dt} = R(T) * 4 * \pi * {r_p}^2 * (1-X_B)^{\frac{2}{3}} = \frac{4*\pi*{r_p}^3*\rho_p}{3*Mr_p} * \frac{dX}{dt} \rightarrow$$

$$\frac{dX}{dt} = \frac{3*Mr_{Mg_2SiO_4}*R(T)*(1-X)^{\frac{2}{3}}}{r_p*\rho_p} \quad (A15)$$

The above equation correlates to the reaction/generation part of the mass balance for a batch reactor. Of course, in the beginning olivine has not reacted and a boundary condition is $X_{initial} = 0$.

From Batch Reactor data to a CSTR Case

When moving to a CSTR case from a BR, the appropriate RTD function and model of molecule mixing have to be taken into consideration, in this case the complete segregation model.

The mean residence time and mean conversion are given respectively by:

$$\bar{\tau} = \frac{V}{F}\ [sec] \quad (2.13)$$

$$\bar{X} = \int_0^\infty X(t) * E(t)\, dt \quad (2.15)$$

The RTD function for a CSTR:

$$E(t) = \frac{1}{\bar{\tau}} * e^{-\frac{t}{\bar{\tau}}} \quad (2.14)$$

Given the volume V of the reactor and the volumetric flow F $\left[\frac{m^3}{sec}\right]$, we can add the "In – Out" term as well, taking into account the inflow and outflow.

Mass balance for reacting olivine:

$$\frac{dX}{dt} = \frac{3 * Mr_{Mg_2SiO_4} * R(T) * (1-X)^{\frac{2}{3}}}{r_p * \rho_p} + \frac{F_{olivine,in} * X_{initial} - F_{out} * X_{final}}{V} \quad (Eq. A15)$$

In the beginning olivine has not reacted and a boundary condition is $X_{initial} = 0$.

Furthermore, $X_{final} = \bar{X}$.

Appendix B – Matlab Codes

- Model

```
% Model for Mineralisation of CO2, Paebbl AB

% Type of reaction: A+B-> C+D
% CO2 + 0.5*Mg2SiO4 --> MgCO3 + 0.5*SiO2

% Below follow 3 cases that can control the conversion of olivine in a Batch
Reactor
% Shrinking Particle Model with:  A. Product/Ash Layer Diffusion Control
%                                 B. Chemical Reaction Control
%                                 C. Film Diffusion Control


% A. Product/Ash Layer Diffusion Control
% 10um, 20um, 50 & 100um particle size comparison


% Given values

r0_A1 = 10*(10^(-6)); % r0 = the radius of the unreacted particle of olivine [m]
r0_A2 = 20*(10^(-6));
r0_A3 = 50*(10^(-6));
r0_A4 = 100*(10^(-6));
rho0 = 3300; % density of olivine [kg/m^3]

C_CO2bulk=60; % Bulk concentration of dissolved CO2 in solution, [kg/m^3]
(provided by Paebbl AB)
C_CO2g=C_CO2bulk;
D_e_CO2= 10^-12; % Effective diffusion coefficient of CO2 through product/ash
layer, [m^2/s]

% Time required for complete dissapearance of a particle, [s]

tau_totalA1=rho0*(r0_A1^2)/(6*1*C_CO2g*D_e_CO2);
tau_totalA2=rho0*(r0_A2^2)/(6*1*C_CO2g*D_e_CO2);
tau_totalA3=rho0*(r0_A3^2)/(6*1*C_CO2g*D_e_CO2);
tau_totalA4=rho0*(r0_A4^2)/(6*1*C_CO2g*D_e_CO2);

% Define the functions

fA1 = @(tA1,X_B1_A1) tA1/tau_totalA1 -1 + 3*(1-X_B1_A1)^(2/3) - 2*(1-X_B1_A1);
fA2 = @(tA2,X_B1_A2) tA2/tau_totalA2 -1 + 3*(1-X_B1_A2)^(2/3) - 2*(1-X_B1_A2);
fA3=  @(tA3,X_B1_A3) tA3/tau_totalA3 -1 + 3*(1-X_B1_A3)^(2/3) - 2*(1-X_B1_A3);
```

```
fA4 = @(tA4,X_B1_A4) tA4/tau_totalA4 -1 + 3*(1-X_B1_A4)^(2/3) - 2*(1-X_B1_A4);

% Set the time interval and initial condition
t0 = 0; X_B10 = 0;
t1f_A1 = tau_totalA1;
t1f_A2 = tau_totalA2;
t1f_A3 = tau_totalA3;
t1f_A4 = tau_totalA4;

% Call the ODE solver function ode89

%10um
optionsA1 = odeset('RelTol',1e-12,'AbsTol',1e-16);
[tA1,X_B1_A1] = ode89(fA1, [t0, t1f_A1], X_B10, optionsA1);

%20um
optionsA2 = odeset('RelTol',1e-12,'AbsTol',1e-16);
[tA2,X_B1_A2] = ode89(fA2, [t0, t1f_A2], X_B10, optionsA2);

%50
optionsA3 = odeset('RelTol',1e-12,'AbsTol',1e-16);
[tA3,X_B1_A3] = ode89(fA3, [t0, t1f_A3], X_B10,optionsA3);

%100
optionsA4 = odeset('RelTol',1e-12,'AbsTol',1e-16);
[tA4,X_B1_A4] = ode89(fA4, [t0, t1f_A4], X_B10,optionsA4);

% Remove the imaginary part of X_B1 using the real function
X_B1_A1 = real(X_B1_A1);
X_B1_A2 = real(X_B1_A2);
X_B1_A3 = real(X_B1_A3);
X_B1_A4 = real(X_B1_A4);

% Define the time range for the polynomial fit
t_A1_fit = tA1(tA1<=1*t1f_A1); % Use 100% of the time range
t_A2_fit = tA2(tA2<=1*t1f_A2); % Use 100% of the time range
t_A3_fit = tA3(tA3<=1*t1f_A3); % Use 100% of the time range
t_A4_fit = tA4(tA4<=1*t1f_A4); % Use 100% of the time range

% Filter the X_B1 values for the selected time range
X_B1_A1_fit = X_B1_A1(tA1<=1*t1f_A1);
X_B1_A2_fit = X_B1_A2(tA2<=1*t1f_A2);
X_B1_A3_fit = X_B1_A3(tA3<=1*t1f_A3);
X_B1_A4_fit = X_B1_A4(tA4<=1*t1f_A4);

% Fit a polynomial equation to the model
pA1 = polyfit(t_A1_fit, X_B1_A1_fit, 9); % Use a ninth-order polynomial
pA2 = polyfit(t_A2_fit, X_B1_A2_fit, 8); % Use a eigth-order polynomial
pA3 = polyfit(t_A3_fit, X_B1_A3_fit, 9); % Use a ninth-order polynomial
pA4 = polyfit(t_A4_fit, X_B1_A4_fit, 12); % Use a twelfth-order polynomial
```

```
% Evaluate the polynomial over the time range
X_B1_A1_fit = polyval(pA1, t_A1_fit);
X_B1_A2_fit = polyval(pA2, t_A2_fit);
X_B1_A3_fit = polyval(pA3, t_A3_fit);
X_B1_A4_fit = polyval(pA4, t_A4_fit);

% Plot the result
figure(1)
plot(tA1, X_B1_A1, 'o', t_A1_fit, X_B1_A1_fit,tA2, X_B1_A2, 'o', t_A2_fit,
X_B1_A2_fit,tA3, X_B1_A3, 'o', t_A3_fit, X_B1_A3_fit,tA4, X_B1_A4, 'o', t_A4_fit,
X_B1_A4_fit)
hold on

% Experimental points for conversion
Experimental_t1 = 3600; % 1h process with 20um particles
Experimental_X1 = 0.344;
Experimental_t2 = 7200; % 2h process with 10um particles
Experimental_X2 = 0.467;
plot(Experimental_t1, Experimental_X1, 'o', 'MarkerSize', 6, 'LineWidth',
2,'Color', [1, 0.5, 0])
plot(Experimental_t2, Experimental_X2, 'o', 'MarkerSize', 6, 'LineWidth', 2)

title('SCM Model of Conversion of Mg_2SiO_4 with Product Layer Diffusion Control',
'FontSize', 14, 'FontWeight', 'bold');
xlabel('Time [s]')
ylabel('X_B')
legend('Model - 10um', 'Polynomial fit - 10um','Model - 20um','Polynomial fit -
20um','Model - 50um','Polynomial fit - 50um','Model - 100um','Polynomial fit -
100um','Experiment 1h - 20um','Experiment 2h - 10um')
ylim([0, 1.01]) % Set y-axis limits to start from 0

set(gca,'XTick',0:1000:tau_totalA4)

% Convert the polynomial coefficients to a string with a custom format
formatSpec = '%+g*t^%d'; % Custom format for polynomial terms

%10um
cA1 = flip(pA1); % Reverse the order of the coefficients
eqnA1 = ''; % Initialize equation string
for i = length(cA1):-1:1
    if cA1(i) ~= 0
        term = sprintf(formatSpec, cA1(i), i-1);
        eqnA1 = [eqnA1 term]; % Add term to equation string
    end
end
eqnA1 = strtrim(eqnA1); % Remove leading space

% Display the equation
fprintf('Polynomial fit equation: %s\n', eqnA1)
% Evaluate the fitted polynomial at t = 300 sec
```

```
t_valA1 = 300; % Set the time value
X_B1_valA1 = polyval(pA1, t_valA1); % Evaluate the fitted polynomial

% Display the result
fprintf('At t = %d, X_B = %f\n', t_valA1, X_B1_valA1);

gA1=eqnA1;

%20um

cA2 = flip(pA2); % Reverse the order of the coefficients
eqnA2 = ''; % Initialize equation string
for i = length(cA2):-1:1
    if cA2(i) ~= 0
        term = sprintf(formatSpec, cA2(i), i-1);
        eqnA2 = [eqnA2 term]; % Add term to equation string
    end
end
eqnA2 = strtrim(eqnA2); % Remove leading space

% Display the equation
fprintf('Polynomial fit equation: %s\n', eqnA2)

% Evaluate the fitted polynomial at t = 500 sec
t_valA2 = 500; % Set the time value
X_B1_valA2 = polyval(pA2, t_valA2); % Evaluate the fitted polynomial

% Display the result
fprintf('At t = %d, X_B = %f\n', t_valA2, X_B1_valA2);

gA2=eqnA2;

%50um

cA3 = flip(pA3); % Reverse the order of the coefficients
eqnA3 = ''; % Initialize equation string
for i = length(cA3):-1:1
    if cA3(i) ~= 0
        term = sprintf(formatSpec, cA3(i), i-1);
        eqnA3 = [eqnA3 term]; % Add term to equation string
    end
end
eqnA3 = strtrim(eqnA3); % Remove leading space

% Display the equation
fprintf('Polynomial fit equation: %s\n', eqnA3)

% Evaluate the fitted polynomial at t = 1000 sec
t_valA3 = 1000; % Set the time value
X_B1_valA3 = polyval(pA3, t_valA3); % Evaluate the fitted polynomial
```

```
% Display the result
fprintf('At t = %d, X_B = %f\n', t_valA3, X_B1_valA3);

gA3=eqnA3;

%100um

cA4 = flip(pA4); % Reverse the order of the coefficients
eqnA4 = ''; % Initialize equation string
for i = length(cA4):-1:1
    if cA4(i) ~= 0
        term = sprintf(formatSpec, cA4(i), i-1);
        eqnA4 = [eqnA4 term]; % Add term to equation string
    end
end
eqnA4 = strtrim(eqnA4); % Remove leading space

% Display the equation
fprintf('Polynomial fit equation: %s\n', eqnA4)

% Evaluate the fitted polynomial at t = 2000 sec
t_valA4 = 2000; % Set the time value
X_B1_valA4 = polyval(pA4, t_valA4); % Evaluate the fitted polynomial

% Display the result
fprintf('At t = %d, X_B = %f\n', t_valA4, X_B1_valA4);

gA4=eqnA4;


% B. Chemical Reaction Control
% 10um, 20um, 50 & 100um particle size comparison

% Set temperature of process

Temperature = 425; %K

% Rate of reaction (Pressure is supposed to be 80Bar-Conversion will be corrected
below)

if (Temperature >= 298) && (Temperature <338)
    Rate = (430+(Temperature-298)/(338-298)*(31600-430))*10^(-11);
elseif (Temperature>=338) && (Temperature<363)
    Rate = (31600+(Temperature-338)/(363-338)*(100000-31600))*10^(-11);
elseif (Temperature>=363) && (Temperature<423)
    Rate = (100000+(Temperature-363)/(423-363)*(1580000-100000))*10^(-11);
elseif (Temperature>=423) && (Temperature<458)
    Rate = (1580000+(Temperature-423)/(458-423)*(6500000-1580000))*10^(-11);
elseif (Temperature>=458 && Temperature<=550)
    Rate = (6500000-(Temperature-458)/(550-458)*6500000)*10^(-11);
```

```
else
    Rate = 0;
end

tau_total2B1=rho0*r0_A1/(1*Rate);
tau_total2B2=rho0*r0_A2/(1*Rate);
tau_total2B3=rho0*r0_A3/(1*Rate);
tau_total2B4=rho0*r0_A4/(1*Rate);

f2B1 = @(tB1,X_B2_B1) (tB1/tau_total2B1) -1 + (1-X_B2_B1)^(1/3);
f2B2 = @(tB2,X_B2_B2) (tB2/tau_total2B2) -1 + (1-X_B2_B2)^(1/3);
f2B3 = @(tB3,X_B2_B3) (tB3/tau_total2B3) -1 + (1-X_B2_B3)^(1/3);
f2B4 = @(tB4,X_B2_B4) (tB4/tau_total2B4) -1 + (1-X_B2_B4)^(1/3);

% Set the time interval and initial condition

t0 = 0; X_B20 = 0;
t2fB1 = tau_total2B1;
t2fB2 = tau_total2B2;
t2fB3 = tau_total2B3;
t2fB4 = tau_total2B4;

%10um
% Call the ODE solver function ode23s
optionsB1 = odeset('RelTol',1e-8,'AbsTol',1e-10);
[tB1,X_B2_B1] = ode23t(f2B1, [t0, t2fB1], X_B20, optionsB1);

%20um
optionsB2 = odeset('RelTol',1e-8,'AbsTol',1e-10);
[tB2,X_B2_B2] = ode23t(f2B2, [t0, t2fB2], X_B20, optionsB2);

%50um
optionsB3 = odeset('RelTol',1e-8,'AbsTol',1e-10);
[tB3,X_B2_B3] = ode23t(f2B3, [t0, t2fB3], X_B20, optionsB3);

%100um
optionsB4 = odeset('RelTol',1e-8,'AbsTol',1e-10);
[tB4,X_B2_B4] = ode23t(f2B4, [t0, t2fB4], X_B20, optionsB4);

%The conversion below accounts for 80 bar. Process was operated at 20 bar
% where evidence suggest that conversion is approximately 50% less compared to
80bar
% Correction : Multiply x2 experimental conversion

% Remove the imaginary part of X_B1 using the real function
X_B2_B1 = real(X_B2_B1);
X_B2_B2 = real(X_B2_B2);
X_B2_B3 = real(X_B2_B3);
X_B2_B4 = real(X_B2_B4);
```

```
% Define the time range for the polynomial fit
t_B1_fit = tB1(tB1<=1*t2fB1); % Use 100% of the time range
t_B2_fit = tB2(tB2<=1*t2fB2); % Use 100% of the time range
t_B3_fit = tB3(tB3<=1*t2fB3); % Use 100% of the time range
t_B4_fit = tB4(tB4<=1*t2fB4); % Use 100% of the time range

% Filter the X_B2 values for the selected time range
X_B2_B1_fit = X_B2_B1(tB1<=1*t2fB1);
X_B2_B2_fit = X_B2_B2(tB2<=1*t2fB2);
X_B2_B3_fit = X_B2_B3(tB3<=1*t2fB3);
X_B2_B4_fit = X_B2_B4(tB4<=1*t2fB4);

% Fit a polynomial equation to the model
pB1 = polyfit(t_B1_fit, X_B2_B1_fit, 3); % Use a third-order polynomial
pB2 = polyfit(t_B2_fit, X_B2_B2_fit, 3); % Use a third-order polynomial
pB3 = polyfit(t_B3_fit, X_B2_B3_fit, 3); % Use a third-order polynomial
pB4 = polyfit(t_B4_fit, X_B2_B4_fit, 3); % Use a third-order polynomial

% Evaluate the polynomial over the time range
X_B2_B1_fit = polyval(pB1, t_B1_fit);
X_B2_B2_fit = polyval(pB2, t_B2_fit);
X_B2_B3_fit = polyval(pB3, t_B3_fit);
X_B2_B4_fit = polyval(pB4, t_B4_fit);

% Plot the result
figure(2)
plot(tB1, X_B2_B1, 'o', t_B1_fit, X_B2_B1_fit,tB2, X_B2_B2, 'o', t_B2_fit,
X_B2_B2_fit,tB3, X_B2_B3, 'o', t_B3_fit, X_B2_B3_fit,tB4, X_B2_B4, 'o', t_B4_fit,
X_B2_B4_fit)
hold on

% Experimental points for conversion
Experimental_t1 = 3600; % 1h process with 20um particles
Experimental_X1 = 0.344;
Experimental_t2 = 7200; % 2h process with 10um particles
Experimental_X2 = 0.467;
plot(Experimental_t1, Experimental_X1, 'o', 'MarkerSize', 6, 'LineWidth',
2,'Color', [1, 0.5, 0])
plot(Experimental_t2, Experimental_X2, 'o', 'MarkerSize', 6, 'LineWidth', 2)

title('SCM Model of Conversion of Mg_2SiO_4 with Chemical Reaction Control',
'FontSize', 14, 'FontWeight', 'bold');
xlabel('Time [s]')
ylabel('X_B')
legend('Model - 10um', 'Polynomial fit - 10um','Model - 20um','Polynomial fit -
20um','Model - 50um','Polynomial fit - 50um','Model - 100um','Polynomial fit -
100um','Experiment 1h - 20um','Experiment 2h - 10um')
ylim([0, 1.01]) % Set y-axis limits to start from 0

set(gca,'XTick',0:1000:tau_total2B4)
```

```
% Convert the polynomial coefficients to a string with a custom format
formatSpec = '%+g*t^%d'; % Custom format for polynomial terms

%10um
cB1 = flip(pB1); % Reverse the order of the coefficients
eqnB1 = ''; % Initialize equation string
for i = length(cB1):-1:1
    if cB1(i) ~= 0
        term = sprintf(formatSpec, cB1(i), i-1);
        eqnB1 = [eqnB1 term]; % Add term to equation string
    end
end
eqnB1 = strtrim(eqnB1); % Remove leading space

% Display the equation
fprintf('Polynomial fit equation: %s\n', eqnB1)

% Evaluate the fitted polynomial at t = 300 sec
t_valB1 = 300; % Set the time value
X_B2_valB1 = polyval(pB1, t_valB1); % Evaluate the fitted polynomial

% Display the result
fprintf('At t = %d, X_B = %f\n', t_valB1, X_B2_valB1);

gB1=eqnB1;

%20um

cB2 = flip(pB2); % Reverse the order of the coefficients
eqnB2 = ''; % Initialize equation string
for i = length(cB2):-1:1
    if cB2(i) ~= 0
        term = sprintf(formatSpec, cB2(i), i-1);
        eqnB2 = [eqnB2 term]; % Add term to equation string
    end
end
eqnB2 = strtrim(eqnB2); % Remove leading space

% Display the equation
fprintf('Polynomial fit equation: %s\n', eqnB2)

% Evaluate the fitted polynomial at t = 500 sec
t_valB2 = 500; % Set the time value
X_B2_valB2 = polyval(pB2, t_valB2); % Evaluate the fitted polynomial

% Display the result
fprintf('At t = %d, X_B = %f\n', t_valB2, X_B2_valB2);

gB2=eqnB2;
```

```
%50um

cB3 = flip(pB3); % Reverse the order of the coefficients
eqnB3 = ''; % Initialize equation string
for i = length(cB3):-1:1
    if cB3(i) ~= 0
        term = sprintf(formatSpec, cB3(i), i-1);
        eqnB3 = [eqnB3 term]; % Add term to equation string
    end
end
eqnB3 = strtrim(eqnB3); % Remove leading space

% Display the equation
fprintf('Polynomial fit equation: %s\n', eqnB3)

% Evaluate the fitted polynomial at t = 1000 sec
t_valB3 = 1000; % Set the time value
X_B2_valB3 = polyval(pB3, t_valB3); % Evaluate the fitted polynomial

% Display the result
fprintf('At t = %d, X_B = %f\n', t_valB3, X_B2_valB3);

gB3=eqnB3;

%100um

cB4 = flip(pB4); % Reverse the order of the coefficients
eqnB4 = ''; % Initialize equation string
for i = length(cB4):-1:1
    if cB4(i) ~= 0
        term = sprintf(formatSpec, cB4(i), i-1);
        eqnB4 = [eqnB4 term]; % Add term to equation string
    end
end
eqnB4 = strtrim(eqnB4); % Remove leading space

% Display the equation
fprintf('Polynomial fit equation: %s\n', eqnB4)

% Evaluate the fitted polynomial at t = 2000 sec
t_valB4 = 2000; % Set the time value
X_B2_valB4 = polyval(pB4, t_valB4); % Evaluate the fitted polynomial

% Display the result
fprintf('At t = %d, X_B = %f\n', t_valB4, X_B2_valB4);

gB4=eqnB4;
```

```
% C. Film Diffusion Control
% 10um, 20um, 50 & 100um particle size comparison

% Time required for complete disappearance of a particle, [s]

tau_total3C1=rho0*r0_A1/(3*1*Rate);
tau_total3C2=rho0*r0_A2/(3*1*Rate);
tau_total3C3=rho0*r0_A3/(3*1*Rate);
tau_total3C4=rho0*r0_A4/(3*1*Rate);

% Define the functions
f3C1 = @(tC1,X_C3_C1) tC1/tau_total3C1 - X_C3_C1;
f3C2 = @(tC2,X_C3_C2) tC2/tau_total3C2 - X_C3_C2;
f3C3 = @(tC3,X_C3_C3) tC3/tau_total3C3 - X_C3_C3;
f3C4 = @(tC4,X_C3_C4) tC4/tau_total3C4 - X_C3_C4;

% Set the time interval and initial conditions

t0 = 0; X_C30 = 0;
t3fC1 = tau_total3C1;
t3fC2 = tau_total3C2;
t3fC3 = tau_total3C3;
t3fC4 = tau_total3C4;

%10um
% Call the ODE solver function ode89
optionsC1 = odeset('RelTol',1e-8,'AbsTol',1e-10);
[tC1,X_C3_C1] = ode89(f3C1, [t0, t3fC1], X_C30, optionsC1);

%20um
optionsC2 = odeset('RelTol',1e-8,'AbsTol',1e-10);
[tC2,X_C3_C2] = ode89(f3C2, [t0, t3fC2], X_C30, optionsC2);

%50um
optionsC3 = odeset('RelTol',1e-8,'AbsTol',1e-10);
[tC3,X_C3_C3] = ode89(f3C3, [t0, t3fC3], X_C30, optionsC3);

%100um
optionsC4 = odeset('RelTol',1e-8,'AbsTol',1e-10);
[tC4,X_C3_C4] = ode89(f3C4, [t0, t3fC4], X_C30, optionsC4);

% Remove the imaginary part of X_C3 using the real function
X_C3_C1 = real(X_C3_C1);
X_C3_C2 = real(X_C3_C2);
X_C3_C3 = real(X_C3_C3);
X_C3_C4 = real(X_C3_C4);

% Define the time range for the polynomial fit
t_C1_fit = tC1(tC1<=1*t3fC1); % Use 100% of the time range
t_C2_fit = tC2(tC2<=1*t3fC2); % Use 100% of the time range
```

```
t_C3_fit = tC3(tC3<=1*t3fC3); % Use 100% of the time range
t_C4_fit = tC4(tC4<=1*t3fC4); % Use 100% of the time range

% Filter the X_B2 values for the selected time range
X_C3_C1_fit = X_C3_C1(tC1<=1*t3fC1);
X_C3_C2_fit = X_C3_C2(tC2<=1*t3fC2);
X_C3_C3_fit = X_C3_C3(tC3<=1*t3fC3);
X_C3_C4_fit = X_C3_C4(tC4<=1*t3fC4);

% Fit a polynomial equation to the model
pC1 = polyfit(t_C1_fit, X_C3_C1_fit, 3); % Use a third-order polynomial
pC2 = polyfit(t_C2_fit, X_C3_C2_fit, 3); % Use a third-order polynomial
pC3 = polyfit(t_C3_fit, X_C3_C3_fit, 3); % Use a third-order polynomial
pC4 = polyfit(t_C4_fit, X_C3_C4_fit, 3); % Use a third-order polynomial

% Evaluate the polynomial over the time range
X_C3_C1_fit = polyval(pC1, t_C1_fit);
X_C3_C2_fit = polyval(pC2, t_C2_fit);
X_C3_C3_fit = polyval(pC3, t_C3_fit);
X_C3_C4_fit = polyval(pC4, t_C4_fit);

% Plot the result
figure(3)
plot(tC1, X_C3_C1, 'o', t_C1_fit, X_C3_C1_fit,tC2, X_C3_C2, 'o', t_C2_fit,
X_C3_C2_fit,tC3, X_C3_C3, 'o', t_C3_fit, X_C3_C3_fit,tC4, X_C3_C4, 'o', t_C4_fit,
X_C3_C4_fit)
hold on

% Experimental points for conversion
Experimental_t1 = 3600; % 1h process with 20um particles
Experimental_X1 = 0.344;
Experimental_t2 = 7200; % 2h process with 10um particles
Experimental_X2 = 0.467;
plot(Experimental_t1, Experimental_X1, 'o', 'MarkerSize', 6, 'LineWidth',
2,'Color', [1, 0.5, 0])
plot(Experimental_t2, Experimental_X2, 'o', 'MarkerSize', 6, 'LineWidth', 2)

title('SCM Model of Conversion of Mg_2SiO_4 with Film Diffusion Control',
'FontSize', 14, 'FontWeight', 'bold');
xlabel('Time [s]')
ylabel('X_B')
legend('Model - 10um', 'Polynomial fit - 10um','Model - 20um','Polynomial fit -
20um','Model - 50um','Polynomial fit - 50um','Model - 100um','Polynomial fit -
100um', 'Experiment 1h - 20um','Experiment 2h - 10um')
ylim([0, 1.01]) % Set y-axis limits to start from 0

set(gca,'XTick',0:200:7200)

% Convert the polynomial coefficients to a string with a custom format
formatSpec = '%+g*t^%d'; % Custom format for polynomial terms
```

```
%10um
cC1 = flip(pC1); % Reverse the order of the coefficients
eqnC1 = ''; % Initialize equation string
for i = length(cC1):-1:1
    if cC1(i) ~= 0
        term = sprintf(formatSpec, cC1(i), i-1);
        eqnC1 = [eqnC1 term]; % Add term to equation string
    end
end
eqnC1 = strtrim(eqnC1); % Remove leading space

% Display the equation
fprintf('Polynomial fit equation: %s\n', eqnC1)

% Evaluate the fitted polynomial at t = 300 sec
t_valC1 = 300; % Set the time value
X_C3_valC1 = polyval(pC1, t_valC1); % Evaluate the fitted polynomial

% Display the result
fprintf('At t = %d, X_B = %f\n', t_valC1, X_C3_valC1);

gC1=eqnC1;

%20um

cC2 = flip(pC2); % Reverse the order of the coefficients
eqnC2 = ''; % Initialize equation string
for i = length(cC2):-1:1
    if cC2(i) ~= 0
        term = sprintf(formatSpec, cC2(i), i-1);
        eqnC2 = [eqnC2 term]; % Add term to equation string
    end
end
eqnC2 = strtrim(eqnC2); % Remove leading space

% Display the equation
fprintf('Polynomial fit equation: %s\n', eqnC2)

% Evaluate the fitted polynomial at t = 500 sec
t_valC2 = 500; % Set the time value
X_C3_valC2 = polyval(pC2, t_valC2); % Evaluate the fitted polynomial

% Display the result
fprintf('At t = %d, X_B = %f\n', t_valC2, X_C3_valC2);

gC2=eqnC2;

%50um

cC3 = flip(pC3); % Reverse the order of the coefficients
```

```
eqnC3 = ''; % Initialize equation string
for i = length(cC3):-1:1
    if cC3(i) ~= 0
        term = sprintf(formatSpec, cC3(i), i-1);
        eqnC3 = [eqnC3 term]; % Add term to equation string
    end
end
eqnC3 = strtrim(eqnC3); % Remove leading space

% Display the equation
fprintf('Polynomial fit equation: %s\n', eqnC3)

% Evaluate the fitted polynomial at t = 1000 sec
t_valC3 = 1000; % Set the time value
X_C3_valC3 = polyval(pC3, t_valC3); % Evaluate the fitted polynomial

% Display the result
fprintf('At t = %d, X_B = %f\n', t_valC3, X_C3_valC3);

gC3=eqnC3;

%100um

cC4 = flip(pC4); % Reverse the order of the coefficients
eqnC4 = ''; % Initialize equation string
for i = length(cC4):-1:1
    if cC4(i) ~= 0
        term = sprintf(formatSpec, cC4(i), i-1);
        eqnC4 = [eqnC4 term]; % Add term to equation string
    end
end
eqnC4 = strtrim(eqnC4); % Remove leading space

% Display the equation
fprintf('Polynomial fit equation: %s\n', eqnC4)

% Evaluate the fitted polynomial at t = 2000 sec
t_valC4 = 2000; % Set the time value
X_C3_valC4 = polyval(pC4, t_valC4); % Evaluate the fitted polynomial

% Display the result
fprintf('At t = %d, X_B = %f\n', t_valC4, X_C3_valC4);

gC4=eqnC4;


display(gA1)
display(gA2)
display(gA3)
display(gA4)
```

```
display(gB1)
display(gB2)
display(gB3)
display(gB4)

display(gC1)
display(gC2)
display(gC3)
display(gC4)
```

- ScaleUp

```
% Scale Up of the Process - Example based on seggregation model
% 5L to 500L for Olivine particle size = 10um

% A+B-> C+D
% CO2 + 0.5*Mg2SiO4 --> MgCO3 + 0.5*SiO2

clear
clc

% Given values
V_reactor = 5*10^-1; % Volume of CSTR reactor [m^3]
F=0.001; % Volumetric flow rate [m^3/sec]
tau_mean=V_reactor/F; % Mean residence time [sec^-1]

syms E t
E=(1/tau_mean)*exp(-t/tau_mean);

display(E)

% g(t)=X(t)*E(t), where X(t) is represented by gA (Product Layer Diffusion
% Control), gB (Chemical Reaction Control) and gC (Film Diffusion Control)
% for the cases of 10um and 50um

syms t

%10um
gA1(t) = ((+1.00769e-24*t^9-4.6702e-21*t^8+9.22525e-18*t^7-1.01322e-
14*t^6+6.77048e-12*t^5-2.83282e-09*t^4+7.38331e-07*t^3-
0.00011722*t^2+0.0118545*t^1-0.0263607*t^0)*E);
gB1(t) = ((+1.78739e-10*t^3-9.54368e-07*t^2+0.00169621*t^1-0.00369213*t^0)*E);
gC1(t) = ((-6.23142e-12*t^3+6.30055e-09*t^2+0.0016901*t^1-0.00154775*t^0)*E);
```

```
%50um
gA3(t) = ((+2.64657e-37*t^9-3.03361e-32*t^8+1.47885e-27*t^7-3.99699e-
23*t^6+6.54768e-19*t^5-6.68279e-15*t^4+4.22296e-11*t^3-1.61961e-
07*t^2+0.000406065*t^1+0.046903*t^0)*E);
gB3(t) = ((+1.43495e-12*t^3-3.81838e-08*t^2+0.000338616*t^1-0.000784564*t^0)*E);
gC3(t) = ((-2.64336e-15*t^3+1.3397e-11*t^2+0.00033837*t^1-0.000330581*t^0)*E);


% Initial condition
a = 0;

%10um
gA1_fun = matlabFunction(gA1); % Convert g functions to a function handle
gB1_fun = matlabFunction(gB1);
gC1_fun = matlabFunction(gC1);

%50um
gA3_fun = matlabFunction(gA3); % Convert g functions to a function handle
gB3_fun = matlabFunction(gB3);
gC3_fun = matlabFunction(gC3);

%10um Mean Conversion
X_meanA1 = integral(gA1_fun, a, inf)
X_meanB1 = integral(gB1_fun, a, inf)
X_meanC1 = integral(gC1_fun, a, inf)

%50um Mean Conversion
X_meanA3 = integral(gA3_fun, a, inf)
X_meanB3 = integral(gB3_fun, a, inf)
X_meanC3 = integral(gC3_fun, a, inf)

if X_meanA1 < 0
    X_meanA1 = 0;
elseif X_meanA1 > 1
    X_meanA1 = 1;
end

if X_meanB1 < 0
    X_meanB1 = 0;
elseif X_meanB1 > 1
    X_meanB1 = 1;
end

if X_meanC1 < 0
    X_meanC1 = 0;
elseif X_meanC1 > 1
    X_meanC1 = 1;
end

if X_meanA3 < 0
```

```
    X_meanA3 = 0;
elseif X_meanA3 > 1
    X_meanA3 = 1;
end

if X_meanB3 < 0
    X_meanB3 = 0;
elseif X_meanB3 > 1
    X_meanB3 = 1;
end

if X_meanC3 < 0
    X_meanC3 = 0;
elseif X_meanC3 > 1
    X_meanC3 = 1;
end

X_meanA1
X_meanB1
X_meanC1
X_meanA3
X_meanB3
X_meanC3
```

Appendix C – Safety Sheet

greenSand

1. IDENTIFICATION OF THE SUBSTANCE AND OF THE COMPANY

CHEMICAL NAME	Magnesium iron silicate
SYNONYMS	greenSand
CAS NO.	1317-71-1
EINECS NO.	215-281-7
APPLICATION	CO2-reduction
VENDOR	Olivine Group / greenSand
POST ADDRESS	Groen van Prinstererstraat 7
	3551 XD Utrecht, the Netherlands
	T. +31 614 236 478

2. COMPOSITION/INFORMATION ON INGREDIENTS

No.	Ingredient name :	Chemical symbol	CAS-no :	Conc. (wt%)	Classifi-cation:
1	Forsterite	Mg_2SiO_4	1317-71-1	94	IK
2	Fayalite	Fe_2SiO_4		6	IK
Legend: T+=Very toxic, T=Toxic, C=Corrosive, Xn=Harmful, Xi=Irritant, IK=No classification required, O=Oxidising, F+=Extremely flammable, F=Very Flammable, N=Dang. to the environment					

None of the ingredients are classified as dangerous.

3. HAZARDS IDENTIFICATION

Not classified as dangerous. greenSand is a natural occurring raw material and is not considered to constitute a health hazard upon normal handling and storage. greenSand contains no free quartz. Inhalation of dust should be avoided as this could irritate the respiratory system.

4. FIRST AID MEASURES

Ingestion:..... Not relevant
Inhalation:..... Remove person from the dust exposed area. Fresh air
Skin contact:..... Wash off with soap and water
Eye contact:..... Rinse immediately with plenty of water, also under the eyelids.
If eye irritation persists, consult a specialist

5. FIRE FIGHTING MEASURES

The material is not flammable. The dust does not constitute an explosion hazard.

6. ACCIDENTAL RELEASE MEASURES

Pick-up and arrange disposal without creating dust. See also point 7, 8 and 13.

7. HANDLING AND STORAGE

Handling: ..... Avoid creating dust
Storage:.....Keep in a dry place

greenSand

8. EXPOSURE CONTROLS/PERSONAL PROTECTION

Regarding occupational exposure the dust is classified as nuisance dust. Exposure limit value for respirable nuisance dust is 4 mg/m3 in the UK. Please check local regulations.
Respiratory protection:..... Use of dust mask, class P2 (EN 149), is recommended
Hand protection: ..... None. Gloves can be used
Eye protection: ..... If necessary, use safety glasses

9. PHYSICAL AND CHEMICAL PROPERTIES

Appearance: ..... Pale-green powder, granaular particles or aggregates
Odour: ..... None
pH: ..... 8,9 – 9,5
Melting range:..... 1400 - 1700°C
Solubility in water: ..... None
Specific density: 3,3 g/cm3
Bulk density: ..... 1,7 - 2,1 g/cm3
Angel of repose: ..... approx. 45°
Stowage factor:..... 0,54 m3 (19 ft3 /t)

10. STABILITY AND REACTIVITY

Hazardous decomposition products: ..... None
Incompatibility with other materials: ..... None

11. TOXICOLOGICAL INFORMATION

Acute oral toxicity: ..... None
Acute dermatol.toxicity: .....None
Inhalation of dust should be avoided as this could irritate the respiratory system.

12. ECOLOGICAL INFORMATION

The product is not characterized as harmful to the environment.

13. DISPOSAL CONSIDERATIONS

May be dumped at approved landfill site. See as well point 7 and 8.

14. TRANSPORT INFORMATION

UN IMDG/IMO ADR/RID ICAO/IATA
- Not subject to classification Not subject to classification Not subject to classification

15. REGULATORY INFORMATION

HEALTH ENVIRONMENT FIRE
CLASSIFICATION CLASSIFICATION CLASSIFICATION
Regarding occupational exposure the dust is classified as nuisance dust. Occupational exposure limit for respirable nuisance dust is 4 mg/m3 in the UK. Please check local regulations in other countries.

16. OTHER INFORMATION

Olivine sand is produced from the rock dunite. In the rock small amounts of fibrous minerals can be found, first of all in the mineral group of inosilicates such as pyroxene and amphiboles.
A normal element analysis (chemical) reports the nickel content as NiO, and may therefore be misleading in showing the form nickel appears in the product. In olivine, nickel is relative strongly bounded in the silicate lattice and thus not bio-available.

The MSDS is prepared according to:
Directive 91/155/EEC, Directive 2001/58/EC and to Directive 2004/73/EC.

For further information: please contact the Olivine Group.